Mineralogical Magazine, December 2014, Vol. 78(7), pp. 1589–1611

Synthetic norsethite, $BaMg(CO_3)_2$: revised crystal structure, thermal behaviour and displacive phase transition

H. EFFENBERGER*, T. PIPPINGER, E. LIBOWITZKY, C. L. LENGAUER AND R. MILETICH

Institut für Mineralogie und Kristallographie, Universität Wien, Althanstrasse 14, 1090 Vienna, Austria

[*Received 19 January 2014; Accepted 18 May 2014; Associate Editor: R. Oberti*]

ABSTRACT

The crystal structure of synthetic $BaMg(CO_3)_2$ whose mineral name is norsethite was re-investigated by single-crystal X-ray diffraction. Complementary *in situ* high- and low-temperature studies by means of vibrational spectroscopy (Raman, IR), powder X-ray diffraction techniques and thermal analyses were performed. Diffraction images (298 K) revealed weak superstructure reflections caused by the displacement of the O atoms in the earlier considered $R\bar{3}m$ structure model (a = 5.0212(9), $c_{\text{new}} = 2\ c_{\text{old}}$ = 33.581(6) Å, $R\bar{3}c$, Z = 6, $R1$ = 0.011, $\sin\theta/\lambda < 0.99$ Å^{-1}). Thermal analyses reveal decarbonatization in two decomposition steps above 750 K, and the heat-flow curves (difference scanning calorimetry) give clear evidence of a weak and reversible endothermal change at 343±1 K. This agrees with a discontinuity in the IR and single-crystal Raman spectra. The changing trend of the *c/a* ratio supports this discontinuity indicating a temperature-induced structural transition in the range between 343 and 373 K. As the change of the unit-cell volume is almost linear, the character of the transition is apparently second order and matches the mechanism of a subtle displacement of the oxygen atom position. The apparent instability of the $R\bar{3}c$ structure is also evidenced by the remarkably larger anisotropic displacement of the oxygen atom.

KEYWORDS: norsethite, space-group symmetry, single-crystal X-ray data, Raman spectroscopy, IR spectroscopy, difference scanning calorimetry, powder X-ray diffractometry, crystal chemistry, non-ambient behaviour, displacive phase transition.

Introduction

WITHIN the scope of a better understanding of the global carbon cycles, carbonate minerals and their structure-property relationships are currently the focus of many studies. Among the simple carbonate minerals, e.g. calcite and aragonite structures, the dolomite series of double carbonates is of particular interest, due specifically to its high flexibility for incorporating divalent cations of various sizes within the crystal structure. An endmember double carbonate phase with cations of very different sizes is the mineral norsethite, $BaMg(CO_3)_2$, where Ba and Mg atoms coexist on the two non-carbon cation sites within the dolomite-related crystal structure. Norsethite is a rare mineral found only at a few localities worldwide, of which the type locality is the Green River formation at the Westvaco Trona mine, Wyoming, USA (Mrose *et al.*, 1961). Further localities include Långban, Sweden (Sundius and Blix, 1965; Åberg and Charalampides, 1988), Rosh Pinah, Namibia (Steyn and Watson, 1967), Chipman Lake, Ontario, Canada (Platt and Wooley, 1990), Tapira, Brazil (Secco and Lavina, 1999), Băiţa, Bihor County, Romania (Onac, 2002), the Jacupiranga alkaline–carbonatite complex, São Paulo State, Brazil (Costanzo *et al.*, 2006), the

---

* E-mail: herta.silvia.effenberger@univie.ac.at
DOI: 10.1180/minmag.2014.078.7.05

Haast River area, New Zealand (Cooper, 1996) and Kovdor on the Kola Peninsula, Russia (Yakovenchuk *et al*., 2006). $BaMg(CO_3)_2$ was also described as an artificial product from slags (Schnorrer *et al.*, 2001).

The early investigations by Mrose *et al.*, (1961) revealed a close structural relationship between norsethite and calcite and dolomite. Nevertheless, the space-group symmetry of norsethite remained unclear and the first precession photographs suggested $R\bar{3}m$, $R3m$, or $R32$ as tentative space groups; $R32$ is suggested as the only possible subgroup on deriving the crystal structure from the calcite-structure type ($R\bar{3}c$). Finally, synthetic norsethite was used for the determination of the crystal structure from X-ray powder data by Lippmann (1968). The author noticed the close fit of the atomic arrangement with space-group symmetry $R\bar{3}m$, but obtained in $R32$ a somewhat lower reliability index, which led him to assume the acentric symmetry to be the true one. A re-investigation using single-crystal data by Effenberger and Zemann (1985) yielded a much clearer picture of the crystal structure of norsethite and verified clearly its relation to dolomite. They confirmed the crystallographic positions of the cations and suggested various models for order and disorder of the oxygen atoms. This involved three models: (1) an ordered model in space group $R\bar{3}m$ (O atoms at the mirror plane, site 18(*h*): x, $\bar{x}$, z); (2) the ordered model favoured by Lippmann (1968) in space group $R32$ (O atoms at site 18(*f*): x, y, z) with x deviating slightly from $\bar{y}$, and (3) a model in $R\bar{3}m$ but with a split oxygen-atom position (O atoms at a half occupied site 36(*i*): x, y, z), again with $x \neq \bar{y}$. In all the three models the Ba and Mg atoms are located unambiguously on the three-fold positions 3(*a*) and 3(*b*), and the carbon atoms are assigned to the site 6(*c*). Limited by the accuracy of measurements at that time, Effenberger and Zemann (1985) gave preference to the ordered model (1) as the most probable for $BaMg(CO_3)_2$. Note that the resulting displacement parameters (particularly U^{11} and U^{22}) of the O atoms were large for all three models and thus did not allow an unambiguous assignment of the true space-group symmetry. More recently Secco and Lavina (1999) studied two natural norsethite samples from a Mg carbonatite and even in that study the question of the true space-group symmetry remained open, although by performing very careful structure investigations and refinements according to the three structure models mentioned, these authors finally also suggested $R\bar{3}m$ as the most probable space group.

New X-ray diffraction technologies and the availability of more sensitive detectors suggested another re-investigation of the crystal structure of synthetic norsethite. The present study reports on this investigation, the somewhat surprising findings and the consequences for the revision of the crystal structure. In addition to the structure determination at ambient temperature we present experimental data of behaviour with temperature variation, as determined by *in situ* measurements using vibrational spectroscopy (Raman from 82 to 473 K and infrared (IR) from 295 to 573 K), difference scanning calorimetry (DSC from 223 to 523 K) and X-ray diffraction techniques (from 100 to 723 K).

Experimental

Sample material

All the investigations for the present study were carried out on the original sample material synthesized and characterized by Lippmann (1968) and later used by Effenberger and Zemann (1985). Individual single crystals as well as polycrystalline powders originate from Lippmann's synthetic single-phase product, which is catalogued under the inventory number 12709a,b in the mineral collection of the Institut für Mineralogie und Kristallographie, Universität Wien. Despite some new finds of natural norsethite during the last few years, material of sufficient crystal quality was not at our disposal and therefore all investigations were performed on the well-characterized sample of synthetic norsethite. Individual euhedral single crystals used for experimental investigations by means of X-ray diffraction and vibrational spectroscopy measure up to a maximum of 50 μm × 50 μm × 100 μm in size, with the longest dimension along the **c** direction of the crystallites.

Single-crystal X-ray diffraction

Single-crystal X-ray diffraction (SXRD) studies at room temperature (298 K) were carried out using a STOE-StadiVari diffractometer system with a Dectris 300K Pilatus pixel-detector. Intensity data collections were performed using a 50 W air-cooled Incoatec IμS microfocus source with a Mo target and high-brilliance 2D-focussing Quazar multilayer mirrors. X-ray data collections at non-ambient temperatures (i.e. T = 100, 150, 200, 250, 293, 320, 330, 340, 350, 360, 370 and 385 K) were performed with a NONIUS kappa diffractometer equipped with a CCD detector (frame size 621 × 576 pixels), a 300 μm capillary-optics collimator, a graphite monochromator, and operated with a conventional sealed-tube Mo source at 30 mA/50 kV power. Temperatures at the sample position were maintained with ±2 K and controlled through a nitrogen-gas cryostream cooler from OXFORD CryoSystems. Based on the data sets recorded with the pixel detector, indexing of reflections revealed clearly the existence of weak superstructure reflections in reciprocal space at positions corresponding to uneven multiples of ½c^*. All structure refinements were carried out corresponding to revised trigonal-cell metrics based on $a \approx 5.0$ Å and $c \approx 33.5$ Å base vectors. Nevertheless, the weak superstructure reflections could not be observed in any of the images taken on the Nonius instrument due to the lower sensitivity of the CCD detector in comparison to the pixel detector. The Bragg intensities including the superstructure reflections are in accordance with the extinction symbol $R_{obv}-c$ suggesting space groups $R3c$ or $R\bar{3}c$. Final convergence in refinement was achieved with a structure model in the space group $R\bar{3}c$. All other refinements were also performed in space group $R\bar{3}c$ with $c \approx 33.5$ Å. Above ~363 K a symmetry change to $R\bar{3}m$ or $R32$ with $c \approx 16.8$ Å is anticipated. Details of the individual diffractometer settings, measurement conditions and crystal-structure refinements performed at various temperatures are compiled in Table 1, resulting structural parameters are given in Table 2, interatomic distances, relevant bond angles and details on polyhedral geometries are listed in Table 3.

Powder X-ray diffraction

Investigations of powder X-ray diffraction (PXRD) were performed in order to obtain cell parameters with greater accuracy. Experimental PXRD measurements were performed on a Bruker D8-Advance diffractometer equipped with a Cu sealed-tube X-ray source, a LynxEye position-sensitive detector, and an Anton Paar XRK900 chamber together with an automated height-compensating alignment stage. The temperature-resolved measurements were performed under 0.5 bar He atmosphere from 298 to 428 K at 5 K, up to 498 K at 10 K and up to 723 K at 25 K intervals. At each temperature the system was allowed to equilibrate for 10 min before a continuous scan over the range 5−75°2θ with an overall counting time of 1 h was performed. Due to the structural characteristics of the doubling of c the intensities of the superstructure reflections with calculated relative intensities <1 were below the detection limit of these PXRD measurements. Recorded data were evaluated using the *TOPAS* software package (Bruker AXS, 2009) applying Pawley-type whole-powder-pattern decomposition (Pawley, 1981) based on the room-temperature symmetry and cell dimensions. The height-compensated displacement factor was proven to be ±25 μm within the desired range. Based on three measurement loops at ten selected temperatures over the chosen temperature range the standard deviations of the cell parameters were determined to be ±0.0005 and ±0.001 Å for a and c, respectively. The accuracy of the sample temperature recording under He is known to be ±2 K. Additionally, the microstructural size and strain characteristics obtained exhibited a constant behaviour of the synthetic $BaMg(CO_3)_2$ investigated up to 648 K. Above this temperature a continuous decrease of the crystallite size together with an increase of the strain could be observed indicating the continuous disintegration reaction starting with the appearance of aragonite-type $BaCO_3$ at 723 K and the disappearance of the title compound at T >798 K.

Vibrational spectroscopy

Confocal micro-Raman experiments were carried out on small individual crystallites. Raman spectra were acquired with a Renishaw RM1000 edge filter-based confocal micro-Raman spectrometer using a 20 mW 632.8 nm HeNe laser for excitation, an objective with a 50-fold magnification as well as a numerical aperture of 0.75, a 1800 mm^{-1} grating, and a thermo-electrically cooled CCD array detector, resulting in a resolution of ~3 cm^{-1}. To reveal minor changes in spectroscopic parameters with temperature, peak-fitting techniques were applied using the program *PeakFit* 4.12 (SeaSolve Software Inc, Massachusetts, USA, 2003), Gauss-Lorentz functions and R^2 > 0.99 in most cases. KBr-diluted and pressed-powder pellets (sample: KBr ~1:200) were chosen as samples for IR investigations. IR spectra were obtained using a Bruker TENSOR27 FTIR spectrometer connected to a Bruker HYPERION FTIR microscope in transmission geometry, using a globar light source, a coated

TABLE 1. Single-crystal X-ray data-collection and structure refinements of norsethite, $BaMg(CO_3)_2$, space group $R\bar{3}c$, $Z = 6$.

Temperature	100 K*	150 K*	200 K*	250 K*	293 K*	320 K*	330 K*	340 K*	350 K*	360 K*	370 K*	385 K*	293 K**
a (Å)	5.0148(9)	5.0153(9)	5.0174(9)	5.0193(9)	5.0212(9)	5.0257(9)	5.0262(9)	5.0277(9)	5.0283(9)	5.0298(9)	5.0294(9)	5.0307(9)	5.021(2)
c (Å)	33.474(6)	33.496(6)	33.516(6)	33.537(6)	33.581(6)	33.592(6)	33.597(6)	33.588(6)	33.595(6)	33.603(6)	33.607(6)	33.617(6)	33.507(16)
c / a	6.675	6.679	6.680	6.682	6.685	6.684	6.684	6.681	6.681	6.681	6.682	6.682	6.673
V (Å^3)	729.0	729.7	730.7	731.7	733.2	734.8	735.0	734.9	735.6	736.2	736.2	736.8	731.6
ρ_{calc} (g cm^{-3}) / μ(Mo$K\alpha$) (mm^{-1})	3.85 / 8.3	3.85 / 8.3	3.84 / 8.2	3.84 / 8.2	3.83 / 8.2	3.82 / 8.2	3.82 / 8.2	3.82 / 8.2	3.82 / 8.2	3.81 / 8.2	3.81 / 8.2	3.81 / 8.2	3.84 / 8.2
Number of images / rotation angle per image (°)	459 / 2	459 / 2	414 / 2	414 / 2	414 / 2	414 / 2	414 / 2	414 / 2	414 / 2	414 / 2	414 / 2	414 / 2	2494 / 0.5
Number of scans	10	10	9	9	9	9	9	9	9	9	9	9	25
Scan time (s/°)	110	110	110	100	110	105	105	105	105	105	105	105	90
Measured reflections	2146	2792	2732	2772	2529	2762	2763	2778	2781	2768	2775	2776	9997
Unique reflections (n) / reflections with $F_o > 4\sigma(F_o)$	319 / 319	318 / 318	319 / 318	318 / 317	318 / 316	323 / 319	324 / 318	322 / 320	324 / 322	325 / 317	323 / 320	324 / 319	681 / 478
$R_{int} = \Sigma\lvert F_o^2 - F_o^2(\text{mean})\rvert / \Sigma F_o^2$	3.71	3.80	4.54	4.13	3.81	4.30	4.39	4.53	4.60	4.54	4.59	4.59	3.19
$R1(\%) = \Sigma(\lVert F_o\rvert - \lvert F_c\rVert) / \Sigma F_o$ (all / observed reflections)	1.44/1.44	1.36/1.36	1.70/1.69	1.54/1.51	1.49/1.44	1.68/1.56	1.82/1.66	1.69/1.66	1.81/1.77	1.90/1.64	1.75/1.67	1.95/1.73	2.65/1.10
$wR2(\%) = [\Sigma w(F_o^2 - F_c^2)^2 / \Sigma\lvert wF_o^4\rvert]^{1/2}$	2.98	2.70	3.18	2.84	2.84	3.27	3.44	3.54	3.58	3.38	3.22	3.54	2.08
Gof = $\{\Sigma[w(F_o^2 - F_c^2)^2] / (n-p)\}^{0.5}$	1.176	1.139	1.182	1.196	1.119	1.157	1.211	1.062	1.207	1.166	1.125	1.143	1.059
Weighting parameters a	0.000	0.000	0.00	0.010	0.010	0.013	0.012	0.020	0.016	0.016	0.016	0.0151	0.010
b	5.20	4.70	5.60	0.70	1.54	1.62	2.00	0.84	0.69	0.29	0.10	1.60	0.00
Final difference Fourier map (min / max heights) (eÅ^{-3})	−1.03/ +1.06	−0.88/ +0.78	−1.24/ +1.30	−1.09/ 0.92	−1.03/ +1.03	−0.62/ +0.71	−0.73/ +0.78	−0.64/ +0.94	−0.59/ +1.09	−0.57/ +0.95	−0.59/ +0.91	−0.65/ +0.98	−0.49/ +0.78

* NONIUS four-circle diffractometer equipped with a CCD detector (frame size 621 × 576 pixels, binned mode) and a 300 μm capillary-optics collimator (Mo tube, graphite monochromator), detector-to-sample distance 30 mm, ω-scan mode; range of data collection ($\pm h \pm k \pm l$): $3° < 2\theta < 80°$. Program: *Collect* (Nonius, 1999; Otwinowski and Minor, 1997). Crystal dimensions: 60 × 50 × 35 μm.

** STOE StadiVari diffractometer equipped with a Pilatus 300 K pixel-detector and a Mo micro-focus X-ray source. Detector-to-sample distance 60 mm. Program: *X-AREA* Version 1.66. (STOE & Cie company, 2013). Crystal dimensions: 60 μm × 30 μm × 20 μm. Range of data collection ($\pm h \pm k \pm l$): $3° < 2\theta < 90°$.

Unit-cell parameters were obtained by least-squares refinements of the 2ω values from the position of all measured reflections. The extinction was found to be below the significance level. Corrections for Lorentz, polarization and absorption effects (multi-scan method) were employed; complex scattering functions (Wilson, 1992) were used; program used for structure refinements: *SHELXL-97* (Sheldrick, 1997, 2008). The value of the maximum shift during the last refinement cycle by the standard deviation (max Δ/σ): < 0.001; the number of variable parameters (p): 17; weighting scheme: $w = 1 / \{\sigma^2(F_o^2) + [a \times P]^2 + b \times P\}$; $P = ([\max(0, F_o^2)] + 2 \times F_c^2) / 3]$.

TABLE 2. Fractional atomic coordinates and displacement parameters of norsethite, $BaMg(CO_3)_2$.

Atom	Position	Wyckoff letter	Site symmetry	Variable parameter	100 K*	150 K*	200 K*	250 K*	293 K*	320 K*	330 K*	340 K*	350 K*	360 K*	370 K*	385 K*	293 K**
Ba	0 0 ¼	6(*a*)	32	U^{11}	0.00609(6)	0.00720(6)	0.00856(7)	0.00990(7)	0.01096(7)	0.01415(7)	0.1438(8)	0.01530(8)	0.01493(8)	0.01531(8)	0.01566(7)	0.01608(8)	0.00847(12)
$U^{11} = U^{22}$; $U^{23} = U^{13} = 0$; $U^{12} = ½\ U^{11}$				U^{33}	0.00831(9)	0.00982(9)	0.01169(11)	0.01414(10)	0.01578(9)	0.01796(10)	0.01834(11)	0.01920(11)	0.01938(12)	0.01979(11)	0.02035(11)	0.02073(12)	0.01219(4)
				U_{equiv}	0.00683(6)	0.00807(5)	0.00960(6)	0.01132(6)	0.01256(6)	0.01542(7)	0.01570(7)	0.01660(7)	0.01641(7)	0.01680(7)	0.0722(7)	0.01763(7)	0.00971(2)
	Principal mean square atomic displacements (Å^2)				0.0083	0.0098	0.0117	0.0141	0.0158	0.0180	0.0183	0.0192	0.0194	0.0198	0.0203	0.0207	0.0122
					0.0061	0.0072	0.0086	0.0099	0.0110	0.0141	0.0144	0.0153	0.0149	0.0153	0.0157	0.0161	0.0085
					0.0061	0.0072	0.0086	0.0099	0.0110	0.0141	0.0144	0.0153	0.0149	0.0153	0.0157	0.0161	0.0085
Mg	0 0 0	6(*b*)	$\bar{3}$	U^{11}	0.0053(3)	0.0055(3)	0.0065(3)	0.0076(3)	0.0077(3)	0.0106(3)	0.0106(3)	0.0118(3)	0.0116(3)	0.0113(3)	0.0119(3)	0.0123(2)	0.00647(10)
$U^{11} = U^{22}$; $U^{23} = U^{13} = 0$; $U^{12} = ½\ U^{11}$				U^{33}	0.0069(5)	0.0081(5)	0.0085(6)	0.0110(5)	0.0123(5)	0.0139(5)	0.0149(5)	0.0151(5)	0.0146(5)	0.0158(5)	0.0155(5)	0.0159(6)	0.0097(2)
				U_{equiv}	0.0058(2)	0.0063(2)	0.0072(2)	0.0087(2)	0.0093(2)	0.0117(2)	0.0120(2)	0.0129(2)	0.0126(2)	0.0128(2)	0.0131(2)	0.0135(2)	0.00753(7)
	Principal mean square atomic displacements (Å^2)				0.0069	0.0081	0.0085	0.0110	0.0123	0.0139	0.0149	0.0150	0.0146	0.0158	0.0155	0.0159	0.0097
					0.0053	0.0055	0.0065	0.0076	0.0077	0.0106	0.0106	0.0118	0.0116	0.0113	0.0119	0.0123	0.0065
					0.0053	0.0055	0.0065	0.0076	0.0077	0.0106	0.0106	0.0118	0.0116	0.0113	0.0119	0.0123	0.0065
C	0 0 *z*	12(*c*)	3	*z*	0.13039(7)	0.13040(7)	0.13044(8)	0.13037(7)	0.13036(7)	0.13032(7)	0.013040(8)	0.13035(7)	0.13029(8)	0.13026(7)	0.13033(7)	0.13040(8)	0.13042(3)
$U^{11} = U^{22}$; $U^{23} = U^{13} = 0$; $U^{12} = ½\ U^{11}$				U^{11}	0.0065(5)	0.0072(5)	0.0087(6)	0.0099(5)	0.0101(5)	0.0123(5)	0.0124(6)	0.0132(6)	0.0135(6)	0.0135(6)	0.0140(5)	0.0145(6)	0.00782(17)
				U^{33}	0.0063(8)	0.0070(8)	0.0071(10)	0.0089(8)	0.0102(8)	0.0121(8)	0.0126(9)	0.0137(9)	0.0127(9)	0.0128(9)	0.0121(8)	0.0143(9)	0.0081(3)
				U_{equiv}	0.0064(4)	0.0071(3)	0.0081(4)	0.0095(4)	0.0101(4)	0.0122(4)	0.0125(4)	0.0133(4)	0.0132(4)	0.0132(4)	0.0133(4)	0.0144(4)	0.00792(12)
	Principal mean square atomic displacements (Å^2)				0.0065	0.0072	0.0086	0.0099	0.0102	0.0123	0.0126	0.0137	0.0135	0.0134	0.0140	0.0145	0.0081
					0.0065	0.0072	0.0086	0.0099	0.0101	0.0123	0.0124	0.0132	0.0135	0.0134	0.0140	0.0145	0.0078
					0.0063	0.0070	0.0071	0.0089	0.0101	0.0120	0.0124	0.0132	0.0127	0.0128	0.0121	0.0143	0.0078
O	*x y z*	36(*f*)	1	*x*	0.1103(6)	0.1110(6)	0.1139(11)	0.1140(9)	0.1145(11)	0.1164(14)	0.1170(16)	0.1168(14)	0.1174(17)	0.1166(13)	0.1163(12)	0.1176(16)	0.11760(19)
				y	−0.1822(6)	−0.1810(6)	−0.1786(11)	−0.1787(9)	−0.1774(11)	−0.1755(14)	−0.1750(16)	−0.1753(14)	−0.1749(17)	−0.1757(13)	−0.1758(12)	−0.1746(16)	−0.17449(19)
				z	0.12931(5)	0.12931(4)	0.12933(5)	0.12934(4)	0.12927(4)	0.12930(5)	0.12927(5)	0.12924(5)	0.12923(5)	0.12921(5)	0.12919(5)	0.12925(5)	0.12926(2)
				U^{11}	0.0138(15)	0.0155(15)	0.020(2)	0.0185(19)	0.020(2)	0.024(3)	0.025(3)	0.025(3)	0.025(3)	0.022(2)	0.022(2)	0.023(3)	0.0240(4)
				U^{22}	0.0118(14)	0.0126(14)	0.017(2)	0.0163(17)	0.0171(19)	0.020(2)	0.020(2)	0.021(2)	0.022(3)	0.020(2)	0.019(2)	0.022(3)	0.0194(4)
				U^{33}	0.0119(5)	0.0142(5)	0.0166(6)	0.0202(6)	0.0229(6)	0.0249(6)	0.0257(6)	0.0274(6)	0.0276(7)	0.0280(6)	0.0280(6)	0.0301(7)	0.0201(2)
				U^{23}	−0.0027(5)	-0.0030(5)	-0.0038(8)	−0.0044(7)	−0.0041(8)	−0.0044(9)	−0.0048(10)	−0.0044(9)	−0.0045(10)	−0.0030(8)	−0.0037(8)	−0.0047(10)	−0.0048(3)
				U^{13}	−0.0040(6)	−0.0049(5)	−0.0064(8)	−0.0073(7)	−0.0080(8)	−0.0083(9)	−0.0084(10)	−0.0082(9)	−0.0082(11)	−0.0071(8)	−0.0080(8)	−0.0088(11)	−0.0081(3)
				U^{12}	0.010(14)	0.0111(14)	0.015(2)	0.0134(18)	0.014(2)	0.016(2)	0.017(3)	0.016(2)	0.017(3)	0.015(2)	0.014(2)	0.016(3)	0.0181(3)
				U_{equiv}	0.0108(6)	0.0123(6)	0.0154(9)	0.0163(8)	0.0178(8)	0.0208(10)	0.0214(11)	0.0221(10)	0.0223(11)	0.0214(10)	0.0215(9)	0.0229(11)	0.01795(15)
	Principal mean square atomic displacements (Å^2)				0.0181	0.0206	0.0266	0.0275	0.0299	0.0334	0.0345	0.0348	0.0352	0.0330	0.0338	0.0365	0.0321
					0.0094	0.0108	0.0134	0.0138	0.0155	0.0180	0.0185	0.0195	0.0199	0.0199	0.0187	0.0200	0.0154
					0.0050	0.0055	0.0063	0.0075	0.0080	0.0110	0.0111	0.0120	0.0116	0.0114	0.0118	0.0123	0.0063

* NONIUS four-circle diffractometer, ** STOE StadiVari four-circle diffractometer.

The anisotropic displacement parameters are defined as: $\exp\left[-2\pi^2\Sigma^3_{i=1}\Sigma^3_{j=1}U_{ij}\ a_i a_j\ h_i\ h_j\right]$.

TABLE 3. Interatomic bond distances (Å), bond angles (°) and crystal chemical data* for norsethite, $BaMg(CO_3)_2$.

	100 K**	150 K**	200 K**	250 K**	293 K**	320 K**	330 K **	340 K**	350 K**	360 K**	370 K**	385 K**	293 K***
Ba atom													
Ba–O, 6 ×	2.796(3)	2.800(3)	2.813(5)	2.815(4)	2.819(5)	2.830(6)	2.831(7)	2.830(6)	2.833(7)	2.830(6)	2.829(5)	2.836(7)	2.8295(9)
Ba–O, 6 ×	3.102(3)	3.099(3)	3.089(5)	3.091(4)	3.087(5)	3.082(6)	3.080(7)	3.080(6)	3.079(7)	3.083(6)	3.083(5)	3.080(7)	3.0725(9)
Δ_{Ba-O}	10.94	10.68	9.81	9.80	9.51	8.90	8.80	8.83	8.68	8.94	8.98	8.60	8.59
O–Ba–O (β_1), 3 ×	67.30(8)	67.24(8)	66.95(14)	66.98(11)	66.86(13)	66.65(17)	66.56(19)	66.52(17)	66.46(19)	66.51(16)	66.53(14)	66.46(19)	66.39(4)
O–Ba–O (β_2), 6 ×	92.60(6)	92.66(6)	92.84(10)	92.82(8)	92.92(9)	93.06(11)	93.12(13)	93.14(11)	93.19(13)	93.15(11)	93.14(10)	93.18(13)	93.23(3)
O–Ba–O (β_3), 3 ×	123.78(6)	123.68(6)	123.71(8)	123.75(6)	123.59(7)	123.54(7)	123.53(8)	123.55(7)	123.54(8)	123.55(7)	123.53(7)	123.56(8)	123.50(3)
O–Ba–O (β_4), 3 ×	137.64(7)	137.70(6)	137.50(8)	137.48(7)	137.56(8)	137.49(9)	137.44(10)	137.40(9)	137.37(10)	137.39(9)	137.42(8)	137.36(10)	137.37(3)
$V_{Voronoi}$	18.61	18.66	18.74	18.77	18.82	18.91	18.92	18.90	18.93	18.92	18.91	18.96	18.84
C.N. (Hoppe)	9.69	9.76	9.94	9.94	10.00	10.13	10.17	10.16	10.19	10.14	10.12	10.21	10.22
C.N. (O'Keeffe)	9.56	9.52	9.69	9.97	9.75	9.89	9.92	9.91	9.95	9.89	9.87	9.96	9.97
Mg atom													
Mg–O, 6 ×	2.0583(15)	2.0602(14)	2.0581(17)	2.0582(15)	2.0633(15)	2.0637(17)	2.0640(18)	2.0638(18)	2.0642(18)	2.0656(17)	2.0664(16)	2.0646(18)	2.0601(7)
O–Mg–O, 6 ×	86.93(6)	86.95(6)	86.87(7)	86.87(6)	86.82(6)	86.85(7)	86.80(7)	86.77(7)	86.75(8)	86.73(7)	86.73(7)	86.76(8)	86.84(3)
O–Mg–O, 6 ×	93.07(6)	93.05(6)	93.13(7)	93.13(6)	93.18(6)	93.15(7)	93.20(7)	93.23(7)	93.25(8)	93.27(7)	93.27(7)	93.24(8)	93.16(3)
σ^2_{oct}	10.28	10.15	10.69	10.69	11.03	10.82	11.17	11.38	11.52	11.66	11.66	11.45	10.89
$V_{Voronoi}$	8.76	8.78	8.76	8.77	8.82	8.83	8.83	8.83	8.84	8.85	8.87	8.84	8.78
C atom													
C–O, 3 ×	1.2835(16)	1.2808(15)	1.2818(18)	1.2828(16)	1.2797(16)	1.2794(18)	1.2798(19)	1.2807(19)	1.2812(20)	1.2821(17)	1.2815(17)	1.2819(20)	1.2787(6)
O–C–O, 3 ×	119.92(1)	119.92(1)	119.92(2)	119.93(1)	119.92(1)	119.93(1)	119.91(2)	119.92(2)	119.92(2)	119.92(1)	119.91(1)	119.91(2)	119.91(1)
O–O, 3 ×	2.222(3)	2.218(3)	2.219(3)	2.221(3)	2.216(3)	2.215(3)	2.216(3)	2.217(3)	2.218(3)	2.220(3)	2.219(3)	2.219(3)	2.2138(10)
Δ_c	0.036(3)	0.036(3)	0.037(3)	0.034(3)	0.037(3)	0.034(3)	0.038(3)	0.037(3)	0.036(3)	0.035(3)	0.038(3)	0.038(3)	0.0390(12)
$V_{Voronoi}$	7.63	7.61	7.64	7.65	7.64	7.65	7.66	7.67	7.68	7.68	7.68	7.69	7.63
C.N. (Hoppe)	3.75	3.75	3.75	3.75	3.75	3.74	3.74	3.74	3.74	3.75	3.75	3.74	3.74
C.N. (O'Keeffe)	3.37	3.37	3.37	3.37	3.36	3.36	3.36	3.36	3.36	3.36	3.36	3.36	3.36
O atom													
O···O	0.3606	0.3511	0.3246	0.3247	0.3158	0.2970	0.2915	0.2941	0.2891	0.2973	0.2992	0.2867	0.2856
$V_{Voronoi}$	13.15	13.16	13.17	13.19	13.21	13.24	13.24	13.24	13.25	13.26	13.26	13.27	13.17
C.N. (Hoppe)	4.60	4.60	4.60	4.60	4.60	4.59	4.59	4.59	4.59	4.59	4.59	4.59	4.59
C.N. (O'Keeffe)	3.37	3.37	3.37	3.37	3.36	3.36	3.36	3.36	3.36	3.36	3.36	3.36	3.36
α	21.92	22.12	22.72	22.73	22.91	23.33	23.46	23.40	23.52	23.34	23.29	23.57	23.58
ε	8.08	7.88	7.28	7.27	7.09	6.67	6.54	6.60	6.48	6.66	6.71	6.43	6.42
μ	8.72	8.80	8.65	8.61	8.76	8.72	8.69	8.68	8.62	8.84	8.69	8.64	8.66
ν	16.15	15.76	14.56	14.55	14.18	13.33	13.08	13.19	12.96	13.32	13.41	12.85	12.83

KBr beam splitter and a liquid nitrogen-cooled MCT detector with a resolution of 4 cm^{-1}. For accurate non-ambient temperature conditions a LINKAM FTIR 600 heating/cooling stage was employed. Unpolarized spectra were acquired in the 40–1800 cm^{-1} range for Raman and in the 550–4000 cm^{-1} range for IR. Thus, the fundamental stretching (ν_1, ν_3) and bending (ν_2, ν_4) vibrations of the carbonate group (~700 to 1450 cm^{-1}) as well as combination and overtone modes (>1450 cm^{-1}) and lattice modes (<400 cm^{-1}) could be obtained (Böttcher *et al.*, 1996, 1997).

Thermoanalytical methods

Difference scanning calorimetry (DSC) measurements were performed on a Mettler DSC821e equipped with a liquid nitrogen cooling device under a continuous flow (50 ml min^{-1}) of dry nitrogen. About 10 mg of ground sample material was prepared in a covered Al crucible. A blank crucible with the equivalent amount of α-corundum powder was used for reference and data were collected between 223 and 523 K at a constant heating rate of 10 K min^{-1}. Three consecutive heating runs were performed on the same sample providing almost identical heatflux curves. Baseline corrections were employed using the equivalent runs of the blank reference crucible. In addition, thermogravimetric analyses (TGA) were performed using a Mettler SDTA851 instrument under dry nitrogen atmosphere (at 25 ml N_2 min^{-1} at 1 bar pressure) in the temperature range 298 to 1373 K at a heating rate of 5 K min^{-1} and sample masses of ~31 mg. Two preliminary heating experiments up to 1023 and 1373 K revealed an incomplete decomposition. Therefore, taking into account the instrumental limitations, an isothermal segment (60 min) at 1373 K was added for the third run. Consecutively each sample material thermally treated was analysed by PXRD.

Results

X-ray crystallography

The most striking feature from inspecting the reciprocal space reconstructed from the 2D X-ray images (recorded with the pixel detector) is the unexpected finding of a superlattice as evidenced by weak superstructure reflections along the **c*** direction. With respect to the base vector lengths of the previously described unit cell ($a \approx 5.0$ Å,

* σ^2_{oct}: bond-angle variance (Fleet, 1976); $\sigma^2_{\mathrm{oct}} = \frac{1}{11}\sum_{i=1}^{12}(\theta_i - 90^\circ)^2$ (θ_i are the individual O–Mg–O bond angles). $\Delta_{\mathrm{Ba-O}}$ (%): difference between the six short and six long Ba–O bond lengths. Δ_{c} (Å): deviation of the C atom from the plane defined by the three O atoms within the carbonate group. V_{Voronoi} (Å^3): volume of the respective Voronoi polyhedron (Program "*KRISTALLCHEMIE*", Nowotny and Zobetz, 1982). C.N. (Hoppe) and C.N. (O'Keeffe): coordination numbers according to Hoppe (1970) and O'Keeffe (1979), respectively; (Program "*KRISTALLCHEMIE*", Nowotny and Zobetz, 1982). O···O (Å): 'splitting' of the O atoms within a carbonate group in space group $R\bar{3}m$. μ (º): rotation angle between top and basic face of the trigonal prismatic $Ba^{[6]}O_6$ polyhedron. ν = 2ε (º): rotation of succeeding carbonate groups due to violation of mirror symmetry but linked by the *c* glide plane. α and α′ (º): angle of the direction of the C–O bond with the face (0110), respectively; α′ = 60º–α. ε = (60º–2α)/2 (º): angle of the direction of the C–O bond with the face $(\bar{1}2\bar{1}0)$ corresponding with the deviation from symmetry $R\bar{3}2/m$ (see text). ** NONIUS four-circle diffractometer. *** STOE StadiVari diffractometer.

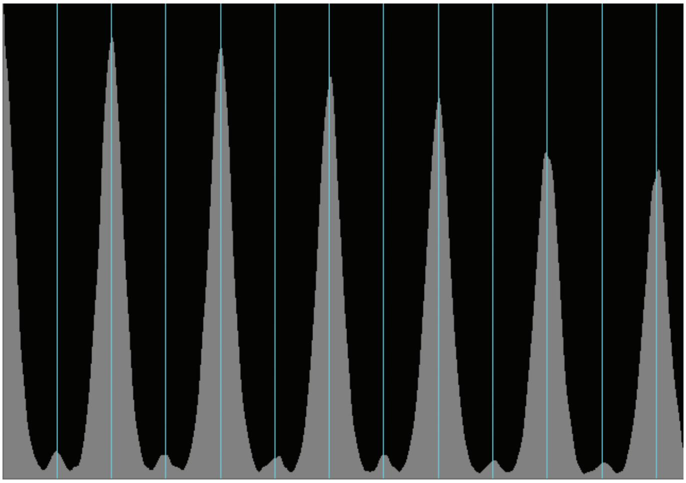

FIG. 1. Direction analysis of the X-ray reflections taken from synthetic norsethite with a Pilatus 300 K pixel-detector mounted on a STOE StadiVari diffractometer system equipped with a Mo microsource indicating clearly the presence of superstructure reflections responsible for the doubled lattice parameter *c*.

$c \approx 16.8$ Å; Effenberger and Zemann, 1985), the analysis of gridlines parallel to the **c*** direction in reciprocal space (Figs 1 and 2) undoubtedly show the existence of additional weak Bragg intensities at uneven multiples of $c^*/2$. The reflection intensities responsible for a doubling of the cell parameter c (= 33.507(16) Å) are weak and visible only in the low 2θ range but exhibit $I_{hkl}/\sigma(I_{hkl})$ ratios up to 7.0; therefore they are considered as significant. Based on a unit-cell setting with $c \approx 33.51$ Å, the indexed intensity data are in accord with the extinction symbol $R_{obv}-c$ suggesting space groups $R3c$ or $R\bar{3}c$ (Fig. 2).

Structure refinements were performed in space groups $R3c$, $R\bar{3}$ and $R\bar{3}c$ for the unit-cell setting with $c \approx 33.51$ Å. Attempts at refinements have also been made with the three structure models (with $c \approx 16.75$ Å) suggested by Effenberger and Zemann (1985), i.e.: (1) with an ordered atomic arrangement in space group $R\bar{3}m$; (2) with an ordered model in space group $R32$; and (3) with a

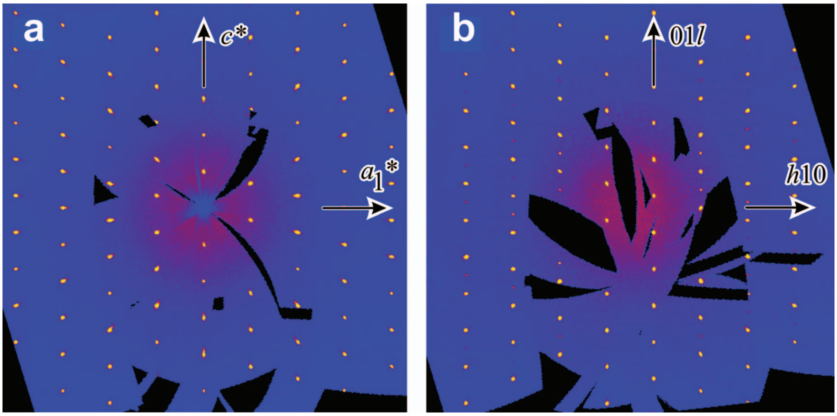

FIG. 2. Reflection images (STOE StadiVari diffractometer system) of synthetic norsethite taken at 293 K. (*a*) Due to the *c* glide plane of space group $R\bar{3}c$ the superstructure reflections in the $h0l$ layer with $l = 2n+1$ are extinguished; (*b*) the $h1l$ reflections exhibit the doubling of the lattice parameter *c* by weak superstructure reflections except in the reciprocal lattice row $\bar{1}1l$ and $01l$ where they are extinguished by the *c* glide plane.

disordered model in space group $R\bar{3}m$ allowing a displacement of the O atom from the mirror plane (split O atom model). The structure model in space group $R\bar{3}c$ and $c \approx 33.51$ Å corresponds with structure model (3) but the doubling of the cell volume results in an ordered model again. The comparison of the refinements of the different models suggests clearly the model in $R\bar{3}c$ with oxygen atoms located on a fully occupied crystallographic site, i.e. the general position 36(*f*). The small but significant differences in the values for the $|x|$ and $|y|$ parameters with respect to the average position $y = \bar{x}$ correspond to an apparent mirror plane, but the values obtained and the uncertainties for both the positional and anisotropic displacement parameters support the revised structure model, which, in addition, agrees with the observed extinction rules; therefore, only this model is considered in the further discussion of stereochemical details.

Raman and IR spectra

Investigations by means of vibrational spectroscopy were performed complementary to the XRD studies to provide additional information on structural features (Scheetz and White, 1977). Figure 3 shows the evolution of Raman spectra in the temperature range from 82 to 473 K. The spectra appear identical at first glance. Even closer inspection does not reveal a discontinuous evolution of bands, either in position or in bandwidth. Similar results are obtained from analogous plots of IR spectra (Fig. 4); due to a windowless setup of the heating/cooling stage in the latter case, temperatures below room temperature were not applicable but the upper limit could be extended to 573 K. To unravel subtle differences in the evolution of spectroscopic parameters with temperature, peak-fitting techniques were applied to determine precise band parameters. Whereas changes of position and full width at half maximum (FWHM) were continuous or even linear in most cases, a number of bands showed a peculiar change in the temperature range of ~353 to 373 K. These changes are definitely beyond any level of uncertainty. Examples of the non-linear evolution of band parameters with temperature as derived from Raman and IR spectra are given in Figs 5 and 6, respectively.

Even though the evolution of Raman band positions of the CO_3 symmetric stretching mode ν_1 at ~1120 cm^{-1} (Fig. 5*a*) is not perfectly smooth at low temperatures, the principal change of the trend at ~373 K is beyond any doubt. Even more impressively, the difference between the positions of the CO_3 symmetric stretching mode ν_1 at ~1120 cm^{-1} and the lattice mode at ~120 cm^{-1} shows a rather drastic change

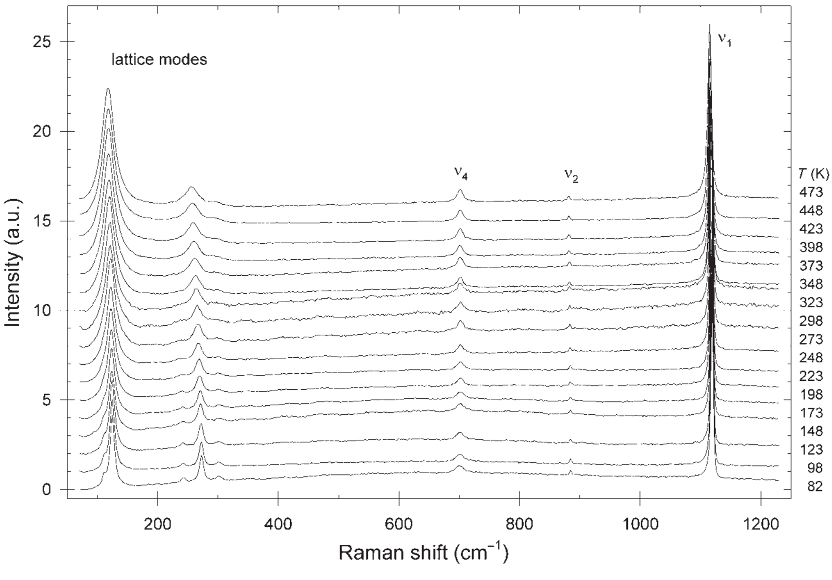

FIG. 3. Raman spectra of synthetic norsethite (offset) from 82 K (lower) to 473 K (upper).

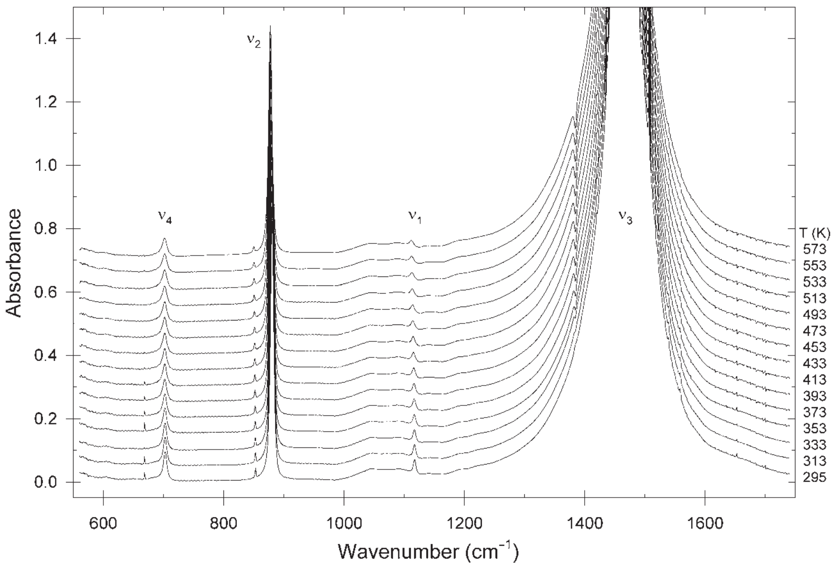

FIG. 4. Infrared spectra of synthetic norsethite (offset) from 295 K (lower) to 573 K (upper).

in the slope (Fig. 5*b*). The non-linear evolution of IR band parameters are rather weak but significant for the CO_3 symmetric stretching mode ν_1 at ~1120 cm^{-1} and the position of the CO_3 overtone or combination band at ~2650 cm^{-1} (Figs 6*a*,*b*). In contrast, the FWHM values of the 880 cm^{-1} IR band of the CO_3 out-of-plane bending mode ν_2 at ~880 cm^{-1} show a more dramatic change at ~333 to 353 K (Fig. 6*c*). The slightly different temperatures may be attributed to a different sample treatment (single-crystal sample *vs.* powdered material in the KBr pellet). Alternatively, running from high to low temperatures, a first indication of deviation from linearity (precursor effect) can be observed as high as 293 K and is emphasized by broken trend lines in Fig. 6*c*. Although the observed changes are mostly faint in terms of absolute values, the non-linear evolution of the relative parameter relationships provides clear evidence for a temperature-induced transformation of the crystal structure of $BaMg(CO_3)_2$.

Raman and IR investigations indicated some temperature-dependent changes in the behaviour of the carbonate group in $BaMg(CO_3)_2$. Even if the suggested phase-transition temperature differs for these two investigations (roughly 373 K and ~333 to 353 K, respectively), the principal presence of a non-linear change concerning some structural details is beyond doubt. A measurement of birefringence (finding the exact wavelength of extinction at a retardation of 15th to 20th order, using a monochromator with $\Delta\lambda$ = ±3.5 nm) *vs*. temperature (295−473 K) revealed a perfectly constant behaviour showed no indication within given uncertainties of a phase transition. Related to the fact that refraction indices depend strongly on changes in density, the absence of any discontinuity in the evolution of the birefringence might be attributed to subtle displacive structural changes, which do not involve significant changes of the unit-cell volume, corresponding to a second-order transition. Moreover, the parallel orientation of the CO_3 groups (which is the very reason for the strong birefringence of all trigonal carbonates), remains unchanged during the transition.

Thermal analyses and decomposition behaviour

Thermogravimetric analyses at constant heating rates were performed in runs up to 1023 and 1373 K, with subsequent analyses of the samples by means of PXRD after cooling to room temperature. The recorded mass curve (Fig. 7) revealed no detectable mass loss up to ~750 K. Between 773 and 943 K synthetic norsethite decomposes with a maximum weight-loss rate at ~880 K. The total weight loss of −16.3(2) wt.% corresponds to the calculated loss of one

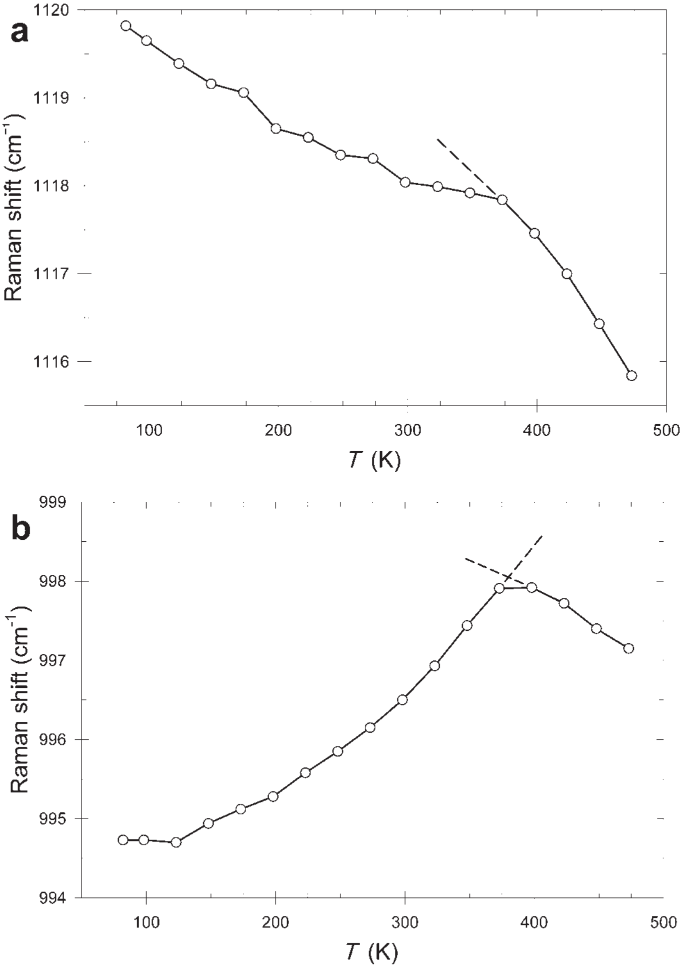

FIG. 5. Non-linear evolution of Raman band parameters of synthetic norsethite from 82 to 473 K. (*a*) Position of the CO_3 symmetric stretching mode ν_1 at ~1120 cm^{-1}. (*b*) Difference between the position of the CO_3 symmetric stretching mode ν_1 at ~1120 cm^{-1} and the lattice mode at ~120 cm^{-1}.

carbonate group per formula unit, i.e. −15.62 wt.%, following the reaction $BaMg(CO_3)_2 \rightarrow BaCO_3 + MgO + CO_2$. The PXRD analysis revealed aragonite-type $BaCO_3$ and X-ray amorphous MgO, with an increasing degree of MgO recrystallization on further annealing of the residual decomposition product. The decarbonatization of $BaCO_3$ was found to start at 1173 K. After the annealing isotherm at 1373 K a cumulative weight loss of −14.3 wt.% was recorded, again almost equivalent to the loss of the remaining CO_2. The PXRD phase analysis of the run product yields crystalline MgO and X-ray amorphous BaO.

The heat-flow curve recorded by DSC clearly reveals evidence of a weak and reversible endothermal change with an onset close to 343±1 K (Fig. 7). This finding correlates with the transition temperature found from the IR investigations, although the thermoanalytical data suggest the transition occurs at a temperature ~30 K lower compared to the Raman investigations. The apparent discrepancies are ascribed to the different type of sample, i.e. in fine-grained powders the transformation is observed at 343 K, while in the single-crystal grains used for Raman spectroscopy the transition is apparently more sluggish due to retardation of heat transfer or

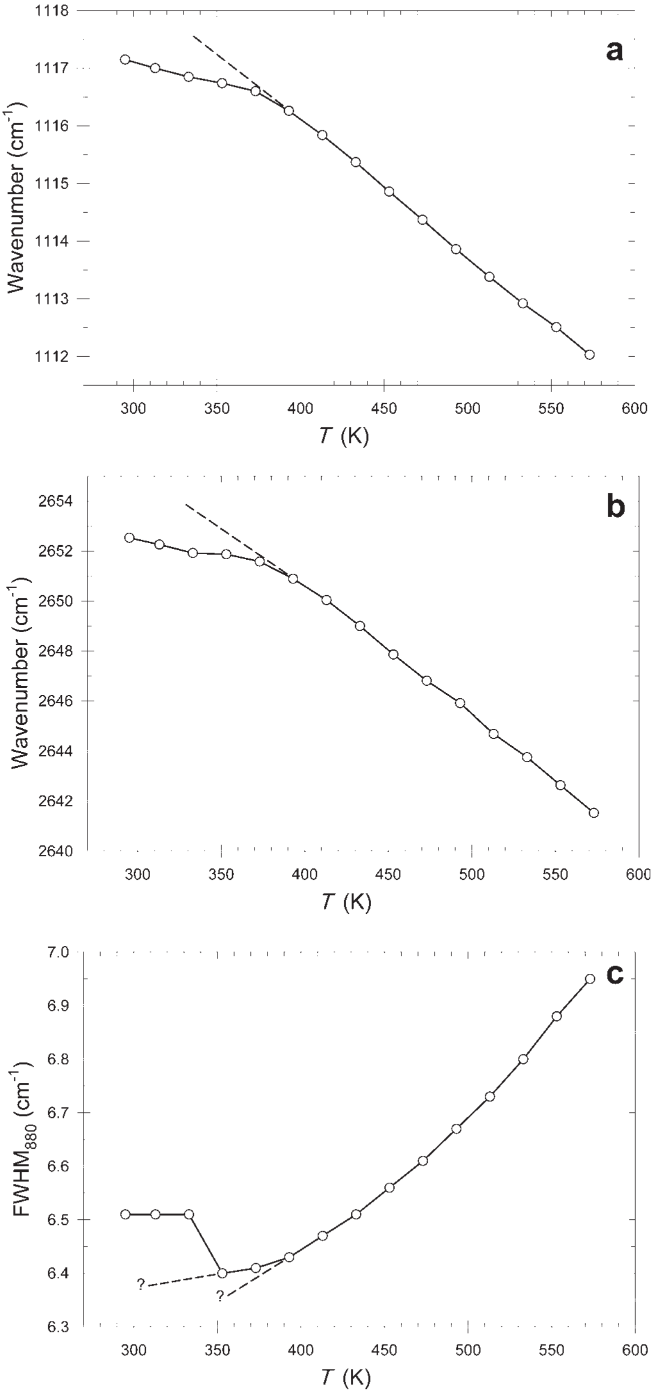

FIG. 6. Non-linear evolution of IR band parameters of synthetic norsethite from 295 to 573 K. (*a*) Position of the CO_3 symmetric stretching mode ν_1 at ~1120 cm^{-1}. (*b*) Position of the CO_3 overtone / combination band at ~2650 cm^{-1}. (*c*) FWHM of the CO_3 out-of-plane bending mode ν_2 at ~880 cm^{-1}.

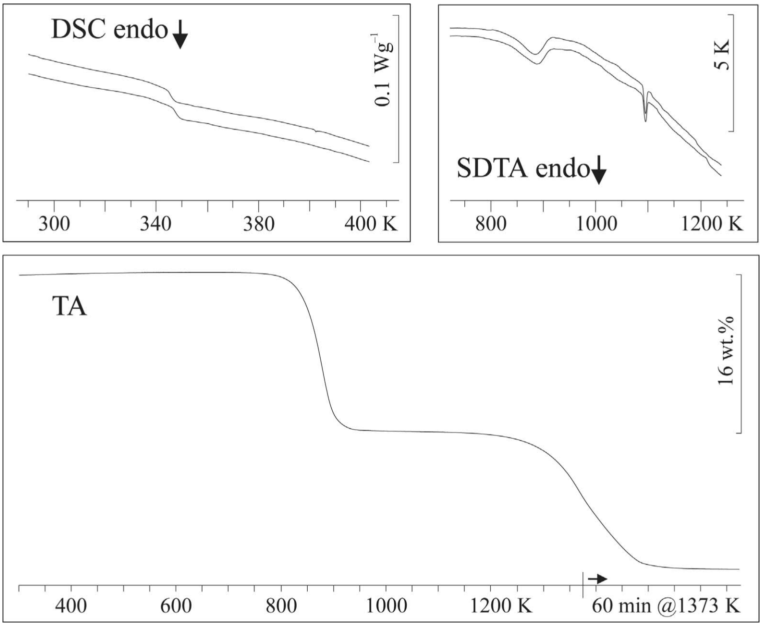

FIG. 7. Thermal analyses of synthetic norsethite. DSC: two consecutive runs of differential scanning calorimetry from 275 to 402 K; SDTA: the signal of two differential thermal analyses from 725 to 1240 K; TA: thermogravimetry of dynamic 300 to 1373 K and 60 min isothermal ranges.

microstructural strain to scale with crystallite size (McKnight *et al*., 2008).

However, all temperature-induced phenomena related to the apparent discontinuity at 343−373 K are weak and consequently structural changes are expected to be small. In contrast, a significant endothermal SDTA signal can be observed with onset temperature at 1078±1 K (Fig. 7), which represents the known *Pmcn* → *R*3*m* phase transition of $BaCO_3$ (Antao and Hassan, 2007). Furthermore, a weak endothermal signal with onset at 1252±2 K indicated the transformation into the cubic, high-temperature modification (Stromme, 1975).

Temperature variations of lattice parameters

X-ray diffraction was used to record the evolution of the lattice dimensions and unit-cell volume with temperature. Within the entire experimentally accessible temperature range (100 to 385 K by SXRD and 298 to 723 K by PXRD) cell parameters *a* and *c* increase with temperature as expected for positive thermal expansion coefficients. However, the evolution with temperature of the cell parameters deviates clearly from linearity (Fig. 8*a*). Changes are even more evident for the *c*/*a* ratios (Fig. 8*b*). Three anisotropic zones and one isotropic zone are apparent: (1) from 100 K to room temperature (*c.f.* Table 1) the cell parameter *c* lengthens more than that of *a*, and the *c*/*a* ratio increases; (2) from room temperature to 333 K, *c*/*a* is almost constant, i.e. the expansion is isotropic; (3) between 333 and 383 K the evolution of *c*/*a* has a negative slope, caused mainly by a reduced expansion along [001]; (4) at temperatures greater than 383 K, a strongly positive evolution is observed until the decomposition temperature of $BaMg(CO_3)_2$. The variation of *c* deviates only slightly from linearity in the region where *c*/*a* increases with temperature, but the gradient of *a* is smaller in this temperature range. The distinct evolution trends of the unit cell do not affect significantly that of the volume, and an almost linear correlation of the V/V_0 ratio with temperature is observed; only a slight increase of the ratio is evident for temperatures above ~400 K (Fig. 8*c*). With the exception of the temperature range between 298 and 383 K, variations of the cell parameters indicate a smaller increase of cell metrics with temperature, i.e. perpendicular to the

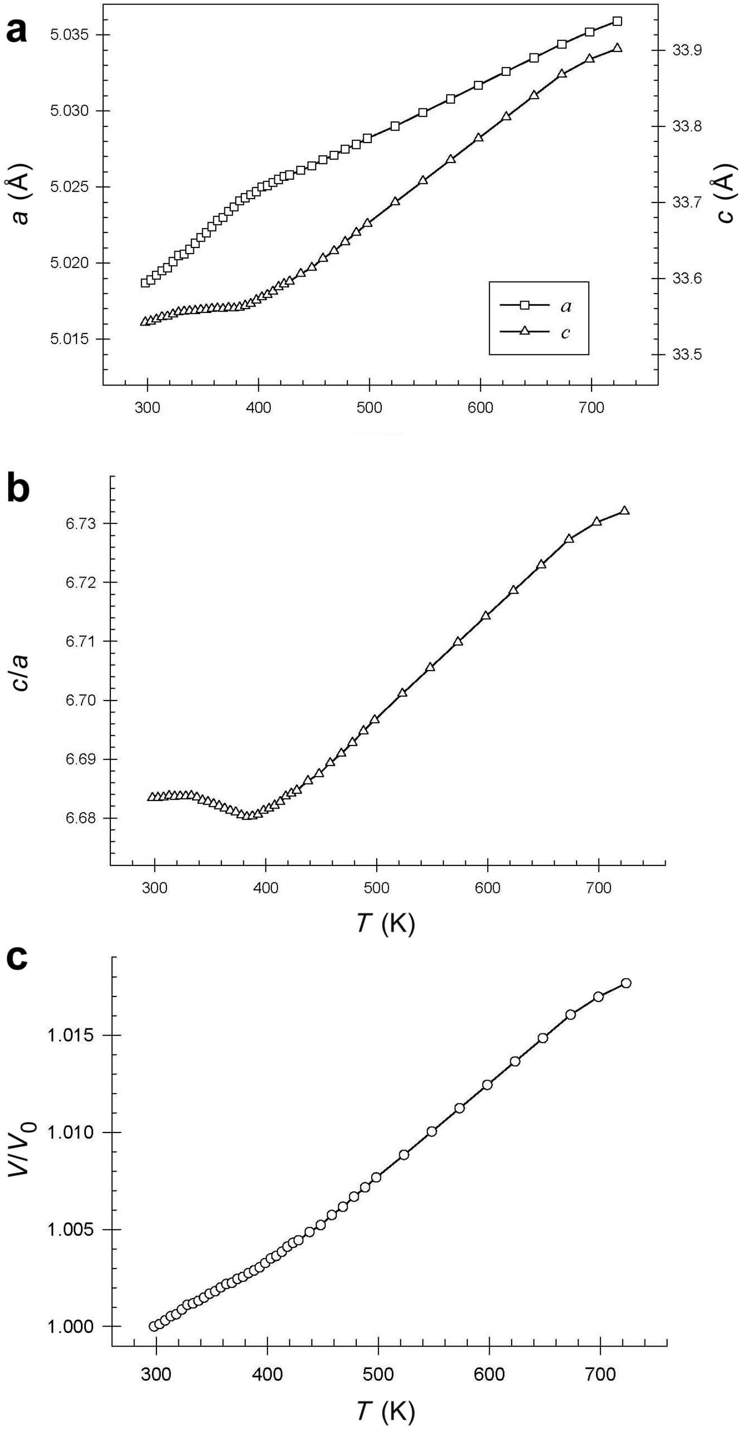

FIG. 8. Variation of the cell metrics of synthetic norsethite in the temperature range 298(2) to 723(2) K as detected by PXRD; (*a*) lattice parameter *a* (± 0.0005 Å) and *c* (± 0.001 Å); (*b*) ratio *c*/*a*; (*c*) V/V_0.

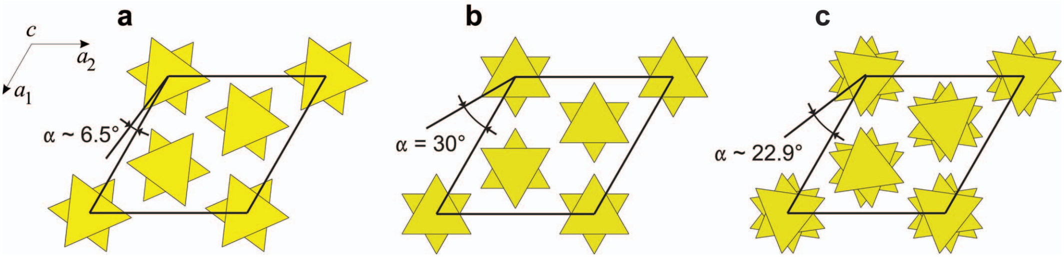

FIG. 9. The orientation of the carbonate group in (*a*) dolomite, space group $R\bar{3}$; (*b*) the structure model of norsethite based on space-group symmetry $R\bar{3}m$ (model 1); and (*c*) structure model of norsethite in space group $R\bar{3}m$ (model 2), $R32$ (model 3), respectively, and in $R\bar{3}c$ but with doubled-cell parameter *c*. The *M* atoms are not indicated; they are below and above the centres of the carbonate groups. (*ATOMS* program; Dowty, 1997).

cation layers (*c.f.* Table 1 and Figs 8 and 9). At approximately room temperature a continuous change of the slope towards to an isotropic decompression is observed, which proceeds to a relative but pronounced shrinkage parallel to the cation layers. This change in the slope is terminated with the critical temperature of the phase transition observed by spectroscopic and DSC investigations. Above the transition point the crystal structure of synthetic norsethite shows again a less pronounced thermal expansion along the **c** direction.

Discussion

Symmetry aspects and the structural relationship to dolomite

The crystal structure of $BaMg(CO_3)_2$ belongs to a group of *R*-centred trigonal double carbonates with two distinct cation positions (*M*1 and *M*2). These cations are arranged in layers parallel to (00.1) with the triangular CO_3 groups interconnecting them. Due to the *R* centring, in each $(n+3)^{th}$ *M* layer alternating *M*1 and *M*2 atoms are stacked exactly above each other, separated by the centre of one carbonate group. The atoms *M*1 and *M*2 exhibit a more or less distorted octahedral coordination. The orientation of the carbonate group is described in Fig. 9*a* (Reeder, 1983). Two mechanisms provide sufficient flexibility to enable the incorporation of atoms of diverse atomic radii on the two *M* sites: (1) a distinct displacement, which shifts the carbonate group parallel to [001] towards either the *M*1 or *M*2 atoms; (2) a moderate rotation of the carbonate group around its triad. The aristotype structure with space-group symmetry $R\bar{3}$ is that of dolomite, $CaMg(CO_3)_2$ (Effenberger *et al.*, 1981, 1983*a*; Reeder and Wenk, 1983; Reeder and Markgraf, 1986; Reeder and Dollase, 1989; Ross and Reeder, 1992; Pilati *et al.*, 1998; Antao *et al.*, 2004; Drits *et al.*, 2005; Zucchini *et al.*, 2012) and the isotypic analogues ankerite, $CaFe(CO_3)_2$ (Beran and Zemann, 1977; Reeder and Dollase, 1989; Ross and Reeder, 1992; Drits *et al.*, 2005), kutnohorite, $CaMn(CO_3)_2$ (Peacor *et al.*, 1987; Farkas *et al.*, 1988; Peacor, 1988*a*,*b*) and minrecordite, $CaZn(CO_3)_2$ (Garavelli *et al.*, 1982). Isotypic borates are known in the natural species nordenskiöldine, $CaSn(BO_3)_2$ (Effenberger and Zemann, 1986) and tusionite, $MnSn(BO_3)_2$ (Kalacheva *et al.*, 1992; Cooper *et al.*, 1994), as well as the synthetic compound $CaSn_{1-x}Ti_x(BO_3)_2$ (Kawano and Yamane, 2010).

When the *M*1 atom has a much larger ionic radius than the *M*2 cation, and may even require a higher coordination number such as with Ba or Pb^{2+} atoms, a significant rotation of the carbonate group allows the coordination polyhedron around the *M*1 atom to increase its coordination number towards [6+6] or [12], while the octahedral coordination of the *M*2 atom is maintained. As a consequence, norsethite, as well as $BaTi(BO_3)_2$ (Zhang *et al.*, 2003; Abdel Khalek *et al.*, 2012) and probably $PbMg(CO_3)_2$ (Lippmann, 1968) also are, strictly speaking, no longer isotypic with dolomite. This apparently also applies to natural and synthetic Mn analogues of norsethite reported by Chang (1964), Hirowatari and Fukuoka (1988), Zidarov *et al.* (2009), Böttcher *et al.* (2012) and Schmidt *et al.* (2013).

A direct comparison between the dolomite structure type and previous descriptions of the norsethite structure type assumed similar base vectors for the trigonal unit cell. Based on this assumption the highest possible symmetry corresponds to space-group symmetry $R\bar{3}m$ with the O atoms located at the mirror plane (Lippmann, 1968; Effenberger and Zemann, 1985; Secco and Lavina, 1999) and thus allowing a regular twelve-fold coordination for the *M*1 atom (Fig. 9*b*). Any deviation of the O atom from the mirror plane results in the formation of a [6+6] coordination around the *M*1 atom (Fig. 9*c*). The rotation angle of the carbonate group as well as the displacement along the **c** direction controls the difference between the shorter and longer *M*1–O bond lengths. Assuming the occupation of one crystallographic site by O atoms, this mechanism is achieved by a dislocation of the O atom from the mirror plane, which in turn requires either a positional disorder when maintaining space-group symmetry $R\bar{3}m$ or symmetry breaking with an atomic displacement off the mirror plane. The latter is accompanied by a reduction of the space-group symmetry to *R*32 (Lippmann, 1968; Effenberger and Zemann, 1985; Secco and Lavina, 1999), whereas Zhang *et al.* (2003) and Abdel Khalek *et al.* (2012) report the centrosymmetric symmetry $R\bar{3}$ for $BaTi(BO_3)_2$.

The whole view is now changed completely due to the knowledge of doubling the *c* axis, which has not been considered previously. This allows the positional shift of the oxygen atoms out of the *pseudo*-mirror plane such that symmetry-equivalent carbonate groups stacked along the **c** direction are alternately rotated clockwise and anti-clockwise. With respect to the doubled periodicity length along the *c* axis the pattern of deliberately rotated carbonate groups follows a *c* glide plane in space group $R\bar{3}c$. Any rotation back to the position resulting in positional parameters with $y = \bar{x}$ would correspond to a true mirror plane parallel to $(1\bar{2}10)$, which in turn requires the halving of the *c* axis length.

Crystal chemistry

According to the refinement of an ordered model in the true space group $R\bar{3}c$, the Ba atom exhibits [6+6] coordination (Fig. 10). The difference between the individual Ba–O bond lengths is ~10% and this decreases with increasing temperature (see Fig. 11*a*). As a result, at higher temperatures the BaO_{12} polyhedron becomes more regular. The arrangement of the six nearest neighbours corresponds to a marginally distorted trigonal prism, with the top and bottom faces twisted against each other by the angle $\mu \approx 8.7°$. Considering the other six ligands, the polyhedral

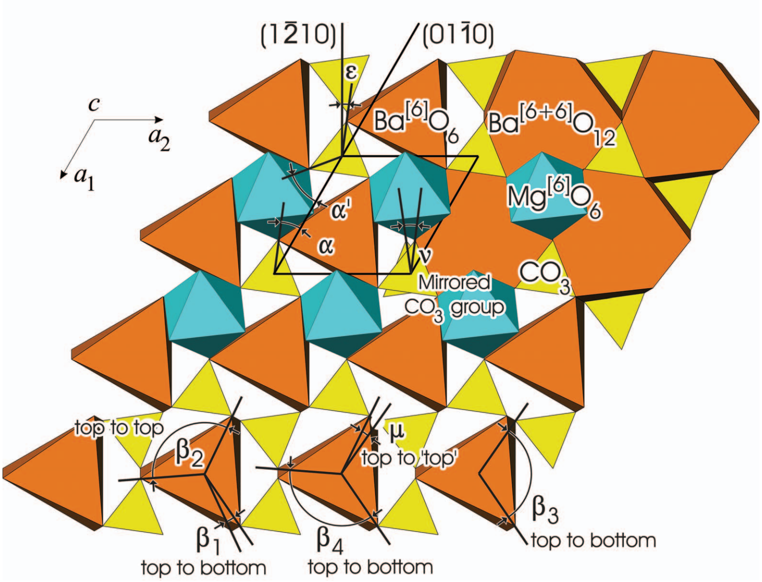

FIG. 10. The crystal structure of synthetic norsethite showing the connection of the Ba atoms with the carbonate groups. Considering the short Ba–O bonds only, trigonal prisms BaO_6 are formed. In the upper right corner the next nearest neighbours are also considered resulting in a distorted ditrigonal prismatic BaO_{12} coordination polyhedron. Some MgO_6 octahedra of the following layer are included. For definition of the angles α (α'), β, ε, μ and ν see Table 3 and text. (*ATOMS* program; Dowty, 1997).

geometry resembles a ditrigonal prism (see Fig. 10). The BaO_{12} polyhedron shares joint edges with the CO_3 groups; considering only the short bonds, the BaO_6 configuration shares only corners with adjacent carbonate groups. The joint O–O edges between the BaO_{12} polyhedron and the CO_3 groups control the shortening and are responsible for the distortion from a regular ditrigonal prismatic geometry. The Ba atom exhibits moderate displacement parameters with the largest elongation parallel to [001] and, as expected, the root mean square (r.m.s.) amplitudes (Fig. 11*b*) increase with increasing temperature.

The O–Ba–O bond angles of the BaO_6 coordination polyhedron vary significantly between 100 and 385 K. The three angles β_1, β_3 and β_4 (all between an O atom in both the top and bottom face; Figs 11*c*,*d*,*f*) decrease with increasing temperature. Only the O–Ba–O bond angles where both O atoms are in the top (or bottom) face alone (β_2) correlate positively with temperature (Fig. 11*e*). This is a result of the relative flattening of the BaO_6 polyhedron with increasing temperature. In contrast, twisting of the top and bottom faces of the trigonal prism (angle μ; *c.f.* Figs 10, 12) is maintained throughout the temperature range investigated. The development of the bond distances results in an increase of the volume of the Voronoi polyhedra as well as an increase of the effective coordination numbers following Hoppe (1970) and O'Keeffe (1979).

The Mg atom is, as expected, octahedrally coordinated and the Mg–O bond-distance variations with temperature are less pronounced (Fig. 13*a*) in comparison to the Ba atom. Bond-distance variations below 250 K do not provide a significant trend, while for the data at T >298 K the expected positive trend can be observed. The O–Mg–O bond angles change continuously and the MgO_6 polyhedron becomes more regular with decreasing temperature as expressed by the bond-angle variance (Fig. 13*b*). The variable distortion is also reflected in the change of the polyhedral volume, and the displacement parameters are moderate, like those for the Ba atom, but they vary on a smaller scale (Fig. 13*c*).

The geometry of the carbonate group in norsethite agrees with the statistics of steric

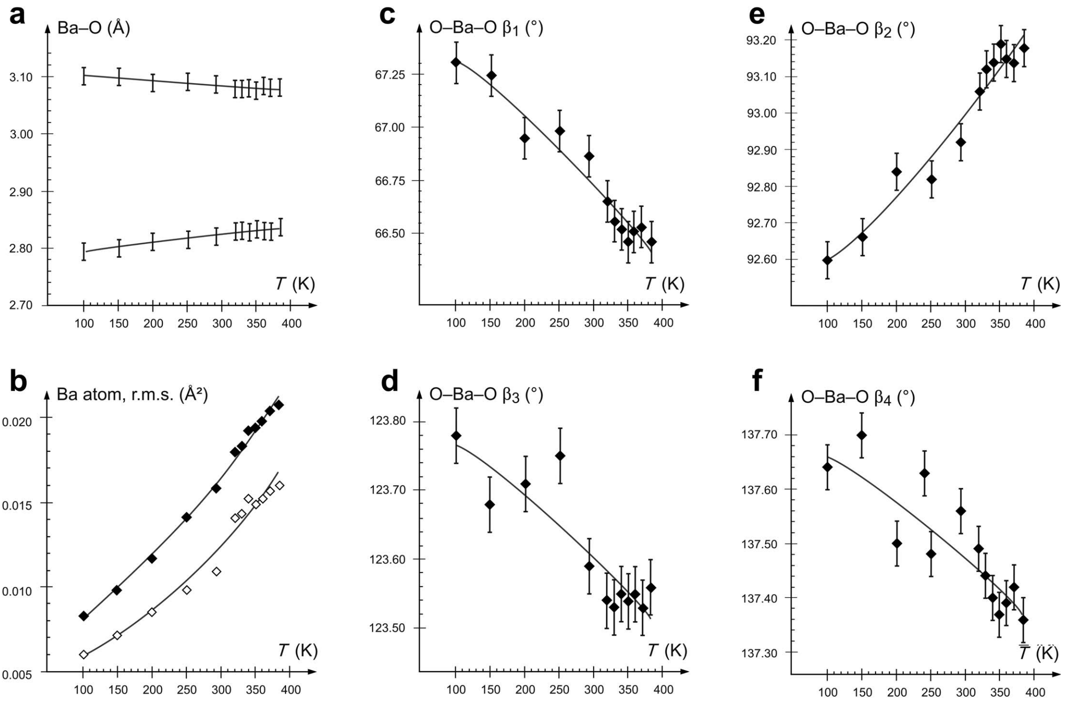

FIG. 11. Variation of the coordination polyhedron around the Ba atom in synthetic norsethite with temperature; (*a*) the Ba–O bond lengths; (*b*) the principal mean-square atomic displacement of the Ba atom; (*c*–*f*) the O–Ba–O bond angles β_1 to β_4 within the BaO_6 polyhedron (for definition see Fig. 10 and text).

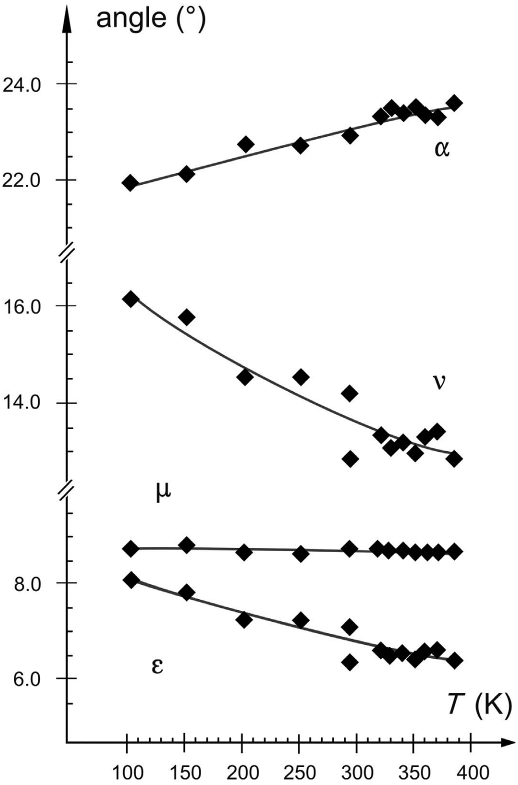

FIG. 12. Characteristic distortion angles of synthetic norsethite; α: angle between the face $(01\bar{1}0)$ and the direction of the C−O bond; ε: angle between the face $(1\bar{2}10)$ and the direction of the C−O bond; μ: rotation between the top and bottom face in the BaO_6 polyhedron; ν: twisting of succeeding carbonate groups linked by the *c* glide plane.

parameters reported by Zemann (1981). Only a minor variability of the C−O bond length from 1.2794(18) to 1.2835(16) Å is observed. The displacement parameters of the C atom increase with temperature. However, the anisotropy of the C atom is insignificant in spite of the almost planar configuration of bonds (Fig. 14*a*). The geometry of the carbonate group is almost invariant within the experimental temperature range. When considering the possibility of changes in the C−O bond lengths and the aplanarity of the carbonate group, no significant changes in temperature variations are identified (*c.f.* Table 3). Figure 14*b* suggests that the *z* coordinate of the C atom might decrease but the *z* coordinate of the O atom shows a similar evolution and compensates for any positional differences between the atoms within the uncertainty of the measurement.

The out-of-plane displacement of the C atom relative to the plane of the three oxygen atoms measures 0.036(3) Å at 298 K, with a positional shift of the C atoms towards the Ba-atom layer. The value of displacement is in agreement with values reported by Effenberger and Zemann (1985) and Secco and Lavina (1999). The deviation from planarity in norsethite is significantly larger compared to those found in other carbonates such as dolomite, ankerite, bütschliite, or rapidcreekite (Effenberger *et al.*, 1981; Drits *et al.*, 2005; Effenberger and Langhof, 1984; Onac *et al.*, 2013), but does not extend to the value reported for thaumasite (Edge and Taylor, 1971; Zemann and Zobetz, 1981; Effenberger *et al.*, 1983*b*; Jacobsen *et al.*, 2003; Gatta *et al.*, 2012).

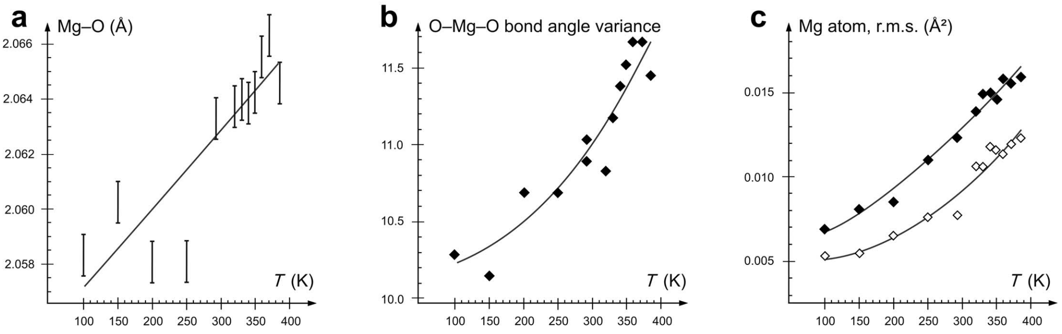

FIG. 13. Variation of the coordination polyhedron around the Mg atom in synthetic norsethite with temperature; (*a*) the Mg−O bond lengths; (*b*) the O−Mg−O bond angle variance (Fleet, 1976); (*c*) the principal mean-square atomic displacement of the Mg atom.

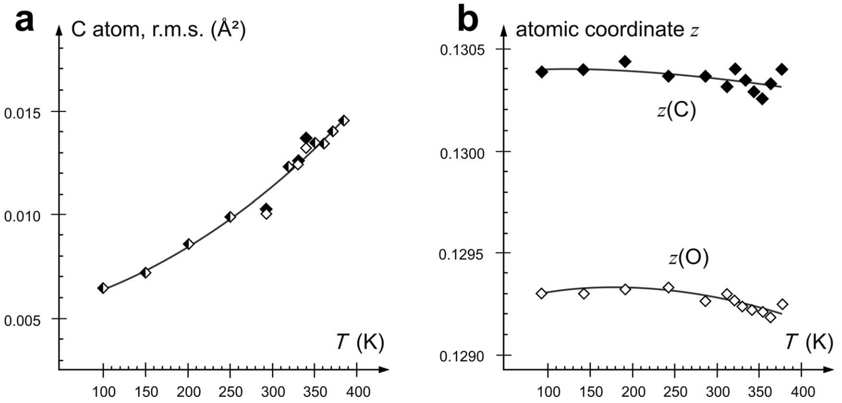

FIG. 14. (*a*) The principal mean-square atomic displacement of the C atom in synthetic norsethite. (*b*) The variation of the atomic coordinate *z* for the C and O atoms.

The oxygen atom and its role in the structural transformation

The location of the oxygen atom is responsible for the differences between the actual and the previously reported models. Moreover it appears most likely to play a crucial role in the subtle changes that are responsible for the weak discontinuities observed by complementary methods. Considering the ordered-structure model with space-group symmetry $R\bar{3}m$, the O atom is located on the mirror plane at $(x,\bar{x},z)$ position. In contrast, the real structure has space-group symmetry $R\bar{3}c$ with the O atom on a general position (x,y,z). With increasing temperature a shift of the O atom towards the fictive mirror plane located in $(1\bar{2}10)$ is evident. The distance between two mirrored O atoms is reduced within the investigated temperature range from 0.3606 Å at 100 K to 0.2867 Å at 385 K (Fig. 15*c*). The corresponding angle ν (Fig. 12) decreases from 16.15º to 12.85º.

Even though the O atom is located at a general position, it exhibits quite large displacement parameters. Both the displacement parameters and the pronounced anisotropy (Fig. 15*d*) correlate clearly with changing temperature. The ratio between the longest axis and the intermediate axes of the 90% probability ellipsoid measures ~2:1 and the ratio between the largest and the smallest axis corresponds to ~3:1, which is above the average anisotropy observed in stable oxygen-based structures. The orientation of the anisotropic ellipsoid indicates a libration of the carbonate group predominantly within the (00.1) plane. At higher temperatures the largest axis of the r.m.s. ellipsoid inclines off the (00.1) plane.

The overall large anisotropy is clear evidence of structural instability and can be interpreted as a prevenient indicator of an impendent structure change. With regard to the observed discontinuities in the vibrational spectra and the clear evidence of a transformation around 343 K from the DSC data, these particular features of the oxygen atom position might support the existence of a transition, which is only driven by the small displacive changes of the oxygen position related to the rotation of the CO_3 group on its threefold axis. Considering that the displacement of the oxygen atom from the fictive mirror plane gets smaller approaching the transition temperature (Fig. 15*c*), a symmetry change from $R\bar{3}c$ to $R\bar{3}m$ (which simultaneously involves halving of the *c* axis and consequently verifies a group–subgroup relation) can be understood easily. The observations suggest the evolution from a crystallographically ordered to an average, possibly dynamically disordered, position of the oxygen atoms in a similar fashion as observed, e.g. for the protons in lawsonite or leonite (Libowitzky and Armbruster, 1995; Hertweck *et al.*, 2001). Nevertheless, due to the technical impossibility of recording the weak superstructure reflections at high temperatures, we cannot yet prove the suggested mechanism from structure refinements.

From spectroscopic and thermal analyses a phase transition is evident at 343 K. The available X-ray data support a phase transition although the experimental proof for the structure of the high-*T* polymorph cannot be given yet. It is evident that

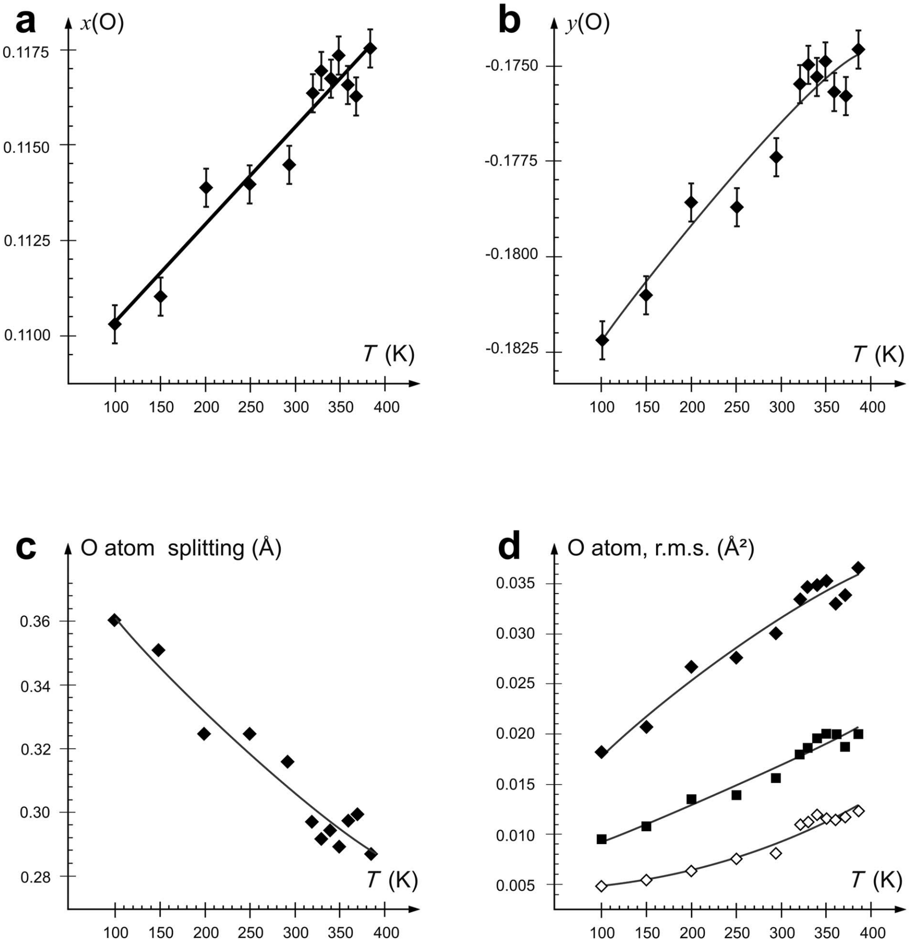

FIG. 15. The O atom in synthetic norsethite; the atomic coordinates (*a*) *x* and (*b*) *y*; (*c*) the splitting of the O atom considering space-group symmetry $R\bar{3}m$ (model 2); and (*d*) the principal mean-square atomic displacements (r.m.s) were recalculated from the anisotropic displacement parameters of the O atom.

the deviation of the O atom from $(1\bar{2}10)$ decreases with increasing temperature (angle ε) and simultaneously the displacement parameters of the O atom and the extent of anisotropy of the thermal displacement give additional evidence for the increasing instability of the $R\bar{3}c$ norsethite structure. It is expected that at this point the weak superstructure reflections responsible for the doubled lattice parameter *c* are most likely to disappear and the structure is best described with a structure model based on space-group symmetry $R\bar{3}m$. Considering the observations that no volume discontinuity accompanies the transformation and that the birefringence, which is very sensitive to any structural changes, remains unchanged across the transition, the given mechanisms of positional displacement of the oxygen atoms suggest clearly that the $R\bar{3}c$ to $R\bar{3}m$ transition is displacive in nature and apparently second order in character.

Acknowledgements

The authors thank Peter Williams (Principal Editor) and the reviewers Fernando Cámara and Giancarlo Della Ventura for their recommendations and comments which improved the manuscript; the manuscript was handled by Associate

Editor, Roberta Oberti. Financial support through start-up funding of the University of Vienna (grant BE532003) and the support of Bruker AXS (Karlsruhe, Germany) are acknowledged.

References

Abdel Khalek, E.K., Mohamed, E.A., Salem, S.M., Ebrahim, F.M. and Kashif, I. (2012) Study of glass-nanocomposite and glass-ceramic containing ferroelectric phase. *Materials Chemistry and Physics*, **133**, 69–77.

Åberg, G. and Charalampides, G. (1988) Evolution of the mineral deposits from Långban, Sweden, as recorded from strontium isotope data. *Geologiska Föreningens i Stockholm Förhandlingar*, **110**, 329–334.

Antao, S.M. and Hassan, I. (2007) $BaCO_3$: high-temperature crystal structures and the *Pmcn* → *R*3*m* phase transition at 811ºC. *Physics and Chemistry of Minerals*, **34**, 573–580.

Antao, S.M., Mulder, W.H., Hassan, I., Crichton, W.A. and Parise, J.B. (2004) Cation disorder in dolomite, $CaMg(CO_3)_2$ and its influence on the aragonite + magnesite - dolomite reaction boundary. *American Mineralogist*, **89**, 1142–1147.

Beran, A. and Zemann, J. (1977) Refinement and comparison of the crystal structures of a dolomite and an Fe-rich ankerite. *Tschermaks Mineralogische und Petrographische Mitteilungen*, **24**, 279–286.

Böttcher, M.E., Gehlken, P.-L. and Reutel, C. (1996) The vibrational spectra of $PbMg(CO_3)_2$. *Neues Jahrbuch für Mineralogie, Monatshefte*, **1996**, 241–250.

Böttcher, M.E., Gehlken, P.-L., Skogby, H. and Reutel, C. (1997) The vibrational spectra of $BaMg(CO_3)_2$ (norsethite). *Mineralogical Magazine*, **61**, 249–256.

Böttcher, M.E., Effenberger, H.S., Gehlken, P.-L., Grathoff, G.H., Schmidt, B.C., Geprägs, P., Bahlo, R., Dellwig, O., Leipe, T., Winde, V., Deutschmann, A., Stark, A., Gallego-Torres, D. and Martinez-Ruiz, F. (2012) $BaMn[CO_3]_2$ – a previously unrecognized double carbonate in low-temperature environments: Structural, spectroscopic, and textural tools for future identification. *Chemie der Erde*, **72**, 85–89.

Bruker AXS (2009) *TOPAS V4.2.2. General profile and structure analysis software for powder diffraction data.* Bruker AXS GmbH, Karlsruhe, Germany.

Chang, L.L.Y. (1964) Synthesis of $MBa(CO_3)_2$ compounds. *American Mineralogist*, **49**, 1142–1143.

Cooper, A.F. (1996) Nb-rich baoite in carbonatites and fenites at Haast River, New Zealand. *Mineralogical Magazine*, **60**, 473–482.

Cooper, M.A., Hawthorne, F.C., Novak, M. and Taylor, M.C. (1994) The crystal structure of tusionite, $Mn^{(2+)}Sn^{(4+)}(BO_3)_2$, a dolomite-structure borate. *The Canadian Mineralogist*, **32**, 903–907.

Costanzo, A., Moore, K.R., Wall, F. and Feely, M. (2006) Fluid inclusions in apatite from Jacupiranga calcite carbonatites: evidence for a fluid-stratified carbonatite magma chamber. *Lithos*, **91**, 208–228.

Drits, V.A., McCarty, D.K., Sakharov, B. and Milliken, K.L. (2005) New insight into structural and compositional variability in some ancient excess-Ca dolomite. *The Canadian Mineralogist*, **43**, 1255–1290.

Dowty, E. (1997) *ATOMS 3.2. A computer program for displaying atomic structures*. Kingsport, Tenessee, USA.

Edge, R.A. and Taylor, F.W. (1971) Crystal structure of thaumasite, $[Ca_3Si(OH)_6{\cdot}12H_2O](SO_4)(CO_3)$. *Acta Crystallographica*, **B27**, 594–601.

Effenberger, H. and Langhof, H. (1984) On the planarity of the CO_3 group in buetschliite, dipotassium calcium dicarbonate, $K_2Ca(CO_3)_2$. *Acta Crystallographica*, **C40**, 1299–1300.

Effenberger, H. and Zemann, J. (1985) Single crystal X-ray investigation of norsethite, $BaMg(CO_3)_2$: one more mineral with an aplanar carbonate group. *Zeitschrift für Kristallographie*, **171**, 275–280.

Effenberger, H. and Zemann, J. (1986) The detailed crystal structure of nordenskiöldine, $CaSn(BO_3)_2$. *Neues Jahrbuch für Mineralogie, Monatshefte*, **1986**, 111–114.

Effenberger, H., Mereiter, K. and Zemann, J. (1981) Crystal structure refinements of magnesite, calcite, rhodochrosite, siderite, smithsonite, and dolomite, with the discussion of some aspects of the stereochemistry of calcite type carbonates. *Zeitschrift für Kristallographie*, **156**, 233–243.

Effenberger, H., Kirfel, A. and Will, G. (1983*a*) Untersuchungen zur Elektronendichteverteilung im Dolomit $CaMg(CO_3)_2$. *Tschermaks Mineralogische und Petrographische Mitteilungen*, **31**, 151–164.

Effenberger, H., Kirfel, A., Will, G. and Zobetz, E. (1983*b*) A further refinement of the crystal structure of thaumasite, $Ca_3Si(OH)_6CO_3SO_4{\cdot}12H_2O$. *Neues Jahrbuch für Mineralogie, Monatshefte*, 60–68.

Farkas, L., Bolzenius, B.H., Schaefer, W. and Will, G. (1988) The crystal structure of kutnohorite $CaMn(CO_3)_2$. *Neues Jahrbuch für Mineralogie, Monatshefte*, 539–546.

Fleet, M.E. (1976) Distortion parameters for coordination polyhedra. *Mineralogical Magazine*, **40**, 531–533.

Garavelli, C.G., Vurro, F. and Fioravanti, G.C. (1982) Minrecordite, a new mineral from Tsumeb. *Mineralogical Record*, **13**, 131–136.

Gatta, G.D., McIntyre, G.J., Swanson, J.G. and Jacobsen, S.D. (2012) Minerals in cement chemistry: A single-crystal neutron diffraction and Raman spectroscopic study of thaumasite, $Ca_3Si(OH)_6(CO_3)(SO_4){\cdot}12H_2O$. *American Mineralogist*, **97**, 1060–1069.

Hertweck, B., Libowitzky, E. and Giester, G. (2001) The crystal structures of the low-temperature phases of leonite-type compounds, $K_2Me(SO_4)_2{\cdot}4H_2O$ (Me^{2+} = Mg, Mn, Fe). *American Mineralogist*, **86**, 1282–1292.

Hirowatari, F. and Fukuoka, M. (1988) Some problems of the studies on the manganese minerals in Japan. *Journal of the Mineralogical Society of Japan*, **18**, 347–365.

Hoppe, R. (1970) Die Koordinationszahl – ein "anorganisches Chamäleon". *Angewandte Chemie*, **82**, 7–16.

Jacobsen, S.D., Smyth, J.R. and Swope, R.J. (2003) Thermal expansion of hydrated six-coordinate silicon in thaumasite, $Ca_3Si(OH)_6CO_3SO_4{\cdot}12H_2O$. *Physics and Chemistry of Minerals*, **30**, 321–329.

Kalacheva, L.V., Yamnova, N.A., Pushcharovskii, D.Y. and Konovalenko, S.I. (1992) Crystal structure of a new natural tusionite borate $MnSn(BO_3)_2$. *Kristallografiya*, **37**, 1557–1558.

Kawano, T. and Yamane, H. (2010) Synthesis, crystal structure and luminescent properties of titanium(IV)-doped calcium borostannates, $CaSn_{1-x}Ti_x(BO_3)_2$. *Journal of Alloys and Compounds*, **490**, 443–447.

Libowitzky, E. and Armbruster, T. (1995) Low-temperature phase transitions and the role of hydrogen bonds in lawsonite. *American Mineralogist*, **80**, 1277–1285.

Lippmann, F. (1968) Die Kristallstruktur des Norsethit, $BaMg(CO_3)_2$. Mit einem Strukturvorschlag für $PbMg(CO_3)_2$. *Tschermaks Mineralogische und Petrographische Mitteilungen*, **12**, 299–318.

McKnight, R.E.A., Moxon, T., Buckley, A., Taylor, P.A., Darling, T.W. and Carpenter, M.A. (2008). Grain size dependence of elastic anomalies accompanying the α-β phase transition in polycrystalline quartz. *Journal of Physics: Condensed Matter*, **20**, 075229.

Mrose, M.E., Chao, E.T.C., Fahey, J.J. and Milton, C. (1961) Norsethite, $BaMg(CO_3)_2$, a new mineral from the Green River formation, Wyoming. *American Mineralogist*, **46**, 420–429.

Nonius, B.V. (1999) *"Collect". Data collection software.* Bruker AXS, Karlsruhe, Germany.

Nowotny, H. and Zobetz, E. (1982) *"KRISTALLCHEMIE". Program for solving geometrical problems in crystal structures.* University of Vienna, Austria.

O'Keeffe, M. (1979) A proposed rigorous definition of coordination number. *Acta Crystallographica*, **A35**, 772–775.

Onac, B.P. (2002) Caves formed within upper Cretaceous skarns at Băiţa, Bihor County, Romania: mineral deposition and speleogenesis. *The Canadian Mineralogist*, **40**, 1693–1703.

Onac, B.P., Effenberger, H.S., Wynn J.G. and Povară, I. (2013) Rapidcreekite in the sulfuric acid weathering environment of Diana Cave, Romania. *American Mineralogist*, **98**, 1302–1309.

Otwinowski, Z. and Minor, W. (1997) Processing of X-ray diffraction data collected in oscillation mode. Pp. 307–326 in: *Methods in Enzymology* (C.W.J. Carter and R.M. Sweet, editors), **276**. AcademicPress, NewYork.

Pawley, G.S. (1981) Unit-cell refinement from powder diffraction scans. *Journal of Applied Crystallography*, **14**, 357–361.

Peacor, D.R. (1988*a*) The crystal structure of kutnahorite $CaMn(CO_3)_2$. *Neues Jahrbuch für Mineralogie, Monatshefte*, **1988**, 539–546.

Peacor, D.R. (1988*b*) The crystal structure of kutnahorite $CaMn(CO_3)_2$. *Powder Diffraction*, **3**, 172–174.

Peacor, D.R., Essene, E.J. and Gaines, A.M. (1987) Petrologic and crystal-chemical implications of cation order-disorder in kutnahorite $CaMn(CO_3)_2$. *American Mineralogist*, **72**, 319–328.

Pilati, T., Demartin, F. and Gramaccioli, C.M. (1998) Lattice-dynamical estimation of atomic displacement parameters in carbonates: calcite and aragonite $CaCO_3$, dolomite $CaMg(CO_3)_2$ and magnesite $MgCO_3$. *Acta Crystallographica*, **B54**, 515–523.

Platt, R.G. and Wooley, A.R. (1990) The carbonatites and fenites of Chipman Lake, Ontario. *The Canadian Mineralogist*, **28**, 241–250.

Reeder, R.J. (1983) Crystal chemistry of the rhombohedral carbonates. Pp. 1–48 in: *Carbonates: Mineralogy and Chemistry* (R.J. Reeder, editor). Reviews in Mineralogy, **11**. Mineralogical Society of America, Washington, DC.

Reeder, R.J. and Dollase, W.A. (1989) Structural variation in the dolomite-ankerite solid-solution series: An X-ray, Moessbauer, and TEM study. *American Mineralogist*, **74**, 1159–1167.

Reeder, R.J. and Markgraf, S.A. (1986) TEM observations and X-ray crystal-structure refinement of a twinned dolomite with a modulated microstructure. *American Mineralogist*, **71**, 795–804.

Reeder, R.J. and Wenk, H.R. (1983) Structure refinement of some thermally disordered dolomites. *American Mineralogist*, **68**, 769–776.

Ross, N.L. and Reeder, R.J. (1992) High-pressure structural study of dolomite and ankerite. *American Mineralogist*, **77**, 412–421.

Scheetz, B.E. and White, W.B. (1977) Vibrational spectra of the alkaline earth double carbonates. *American Mineralogist*, **62**, 36–50.

Schmidt, B.C., Gehlken, P.-L. and Böttcher, M.E. (2013) Vibrational spectra of $BaMn(CO_3)_2$ and a re-analysis of the Raman spectrum of $BaMg(CO_3)_2$. *European Journal of Mineralogy*, **25**, 137–144.

Schnorrer, G., Stahlmann, W. and Möllenkamp, A. (2001) Sekundärmineralisation in den

Hochofenschlacken des Hüttenwerkes in Georgsmarienhütte, heute Georgsmarienhütte GmbH. *Der Aufschluβ*, **52**, 99−108.

Secco, L. and Lavina, B. (1999) Crystal chemistry of two natural magmatic norsethites, $BaMg(CO_3)_2$, from an Mg-carbonatite of the alkaline carbonatitic complex of Tapira (SE Brazil). *Neues Jahrbuch für Mineralogie, Monatshefte*, **1999**, 87−96.

Sheldrick, G.M. (1997) *SHELXL-97, a program for crystal structure refinement.* University of Göttingen, Germany.

Sheldrick, G.M. (2008) A short history of SHELX. *Acta Crystallographica*, **A64**, 112−122.

Steyn, J.G.D. and Watson, M.D. (1967) A new occurrence of norsethite, $BaMg(CO_3)_2$. *American Mineralogist*, **52**, 1770−1775.

STOE & Cie Company (2013) *X-AREA, Version 1.66, Stadi Vari Pilatus*. Darmstadt, Germany.

Stromme, K.O. (1975) On the crystal structures of the high-temperature forms of strontium and barium carbonate and structurally related compounds. *Acta Chemica Scandinavia*, **A29**, 105−110.

Sundius, N. and Blix, R. (1965) Norsethite from Långban. *Arkiv för Mineralogi och Geologi*, **4**, 277−278.

Wilson, A.J.C. (editor) (1992) *International Tables for Crystallography, Vol. C., Mathematical, Physical and Chemical Tables*. Kluwer Academic Press, Dordrecht, The Netherlands.

Zemann, J. (1981) Zur Stereochemie der Karbonate. *Fortschritte in Mineralogie*, **59**, 95 −116.

Zemann, J. and Zobetz, E. (1981) Do the carbonate groups in thaumasite have anomalously large deviations from coplanarity? *Kristallografija*, **26**, 1215−1217.

Yakovenchuk, V.N., Ivanyuk, G.Y., Mikhailova, Y.A., Selivanova, E.A. and Krivovichev, S.V. (2006) Pakhomovskyite, $Co_3(PO_4)_2{\cdot}8H_2O$, a new mineral species from Kovdor, Kola Peninsula, Russia. *The Canadian Mineralogist*, **44**, 117−123.

Zhang, S.-Y., Wu, X., Chen, X.-L., He, M., Cao, Y.G., Song, Y.T. and Ni, D.Q. (2003) Phase relations in the $(BaO)-(B_2O_3)-(TiO_2)$ system and the crystal structure of $BaTi(BO_3)_2$. *Material Research Bulletin*, **38**, 783−788.

Zidarov, N., Petrov, O., Tarassov, M., Damyanov, Z., Tarassova, E., Petkova, V., Kalvachev, Y. and Zlatev, Z. (2009) Mn-rich norsethite from the Kremikovtsi ore deposit, Bulgaria. *Neues Jahrbuch für Mineralogie, Abhandlungen*, **186**, 321−331.

Zucchini, A., Comodi, P., Katerinopoulou, A., Balic Zunic, T., McCammon, C. and Frondini, F. (2012) Order-disorder-reorder process in thermally treated dolomite samples: a combined powder and single-crystal X-ray diffraction study. *Physics and Chemistry of Minerals*, **39**, 319−328.